nature portfolio

Peer Review File

Unlocking the Capacity of Mn-based Prussian Blue Cathodes in Capacitive Deionization

Corresponding Author: Professor Gang Wang

This file contains all reviewer reports in order by version, followed by all author rebuttals in order by version.

Version 0:

Reviewer comments:

Reviewer #1

(Remarks to the Author)
This manuscript describes the design and electrochemical investigation of a K^+-substituted high-entropy Prussian blue analogue (K-HEHCF) for enhanced capacitive deionization and energy recovery applications. The authors systematically analyze the structural stabilization effects induced by both high configurational entropy and K^+ substitution, demonstrating improved water resistance, lattice stability, and energy recovery efficiency compared to conventional HEHCFs. The manuscript is well organized, and the experimental data are comprehensive and clearly presented.

1. While the manuscript is well executed, the originality of the work is somewhat limited. The authors have previously reported a high-entropy PBA system in Advanced Science (2024) (Ref. 35), and the present study appears to be an extension of that concept through the incorporation of K^+ substitution. However, the effects of K^+ ions on PBA frameworks—such as water-content reduction, structural stabilization, and partial ion-exchange behavior—have already been well documented in the literature. In particular, K^+-substituted HE-PBAs have recently been reported in Desalination (617 (2026) 119487). Therefore, the distinct contribution of this study should be more clearly emphasized.

2. The manuscript frequently attributes the superior performance of K-HEHCF to the synergistic effect between high configurational entropy and K^+ incorporation. However, this synergy has not been rigorously validated, as the two factors are not experimentally decoupled.

3. To generalize the proposed mechanism, the authors are encouraged to compare the K^+ substitution behavior in other metal-centered PBAs (e.g., Co–HCF, Ni–HCF, or Fe–HCF). This would help clarify whether the observed “pillar effect” and water-content suppression are universal phenomena or specific to Mn-based systems.

4. The CDI performance is impressive, but additional quantitative metrics are necessary to assess the practical feasibility of the proposed system. Specifically, the following data are recommended:
- Energy consumption per mole of salt removed (kWh mol^{-1} or kWh m^{-3}).
- Long-term electrode lifetime and structural stability beyond 200 cycles.
- Coulombic efficiency and true energy recovery ratio during charge/discharge cycles.

Reviewer #2

(Remarks to the Author)
In this manuscript, K-based high entropy hexacyanoferrate (K-HEHCF) is successfully synthesized by a one-step co-precipitation method. This electrode material can achieve good electrical conductivity and stability. The successful synthesis of the electrode material was demonstrated by various characterizations, and good desalination performance can be achieved in CDI applications. However, the experimental content of this manuscript is not novel enough, the materials are not innovative, so it cannot be accepted. The following are rejection reasons.

1.Please give the contents of different elements in K-HEHCF and Na-HEHCF to prove the mole fractions of the five elements are close to each other with about 0.2 using ICP and calculate the configuration entropy to ensure that $\Delta S_{conf} > 1.5R$.

2.The pseudo-capacitance calculation results of electrochemical tests show that the capacitance contribution rate of K-HEHCF increases from 34.4% to 81.6%. Why does this part of the data show that the proportion of capacitance is relatively small? Please explain and modify it. Please re-select the small sweep speed range and calculate the capacitance contribution more convincingly.
3.Why the K-HEHCF have good removal efficiency for the common multivalent salt ions, especially for Ca2+?
4.Please compare the contents of K and Na in materials before and after cycling to prove the exchange of K and Na during the reaction process. “Part of K+ will stay in K-HEHCF to be the backbone”. Will this part K+ gradually decrease during long-term cycling, or will it remain in the material during long-term cycling? Please confirm it.
5.There are several similar published papers like https://doi.org/10.1021/acsnano.3c02323; https://doi.org/10.1007/s12274-022-5020-0; https://advanced.onlinelibrary.wiley.com/doi/10.1002/adfm.202510533.
6.What is the mass of K-HEPBA and AC electrode respectively? In the desalination test, an area of 4.5*6.5 cm2 is used, and the desalination performance test is greatly affected by the mass and area of the electrode, so please fully compare the desalination capacity of HEPBA with different mass and area.

Version 1:

Reviewer comments:

Reviewer #1

(Remarks to the Author)
The manuscript has been revised satisfactorily in accordance with the comments. It may be accepted for publication in Nature Communications.

Reviewer #2

(Remarks to the Author)
Although the authors have addressed several previous comments, there remain significant concerns regarding the electrochemical characterization and computational analysis sections. These issues are fundamental and must be resolved before the manuscript can be considered for publication. The main reasons for rejection are outlined below:
1. According to the Methods section, the cyclic voltammetry (CV) measurements were conducted using a three-electrode system in 1 M NaCl, with scans performed from low to high voltage. However, in Figures 3a and 3b, the positions of the oxidation and reduction peaks are reversed compared with those reported in previous publications on HEPBA and PBA materials. Please clarify and explain this discrepancy. Furthermore, in Figure 3f, the galvanostatic charge–discharge (GCD) curve shows the oxidation peak as higher than the reduction peak, which is inconsistent with the CV profiles. please provide a clear explanation of this inconsistency and verify the accuracy of electrochemical data.
2. The manuscript lacks a dedicated Methods section describing the density functional theory (DFT) calculations. To ensure reproducibility and technical reliability, please add detailed information on the computational approach used. In addition, the raw computational input files and key output files should be provided for all critical points and transition states discussed in the text.
3. For the adsorption energy study shown in Figure 5h, the optimized adsorption structure of Na-PBA should be provided. Regarding Figure 5i, the current number of images used is insufficient to accurately fit the reaction pathway, particularly for the green line. The authors should recompute the results using an adequate number of intermediate states and include the corresponding energy barrier values along with fully optimized atomic structures for the initial, intermediate, and final configurations.

Version 2:

Reviewer comments:

Reviewer #2

(Remarks to the Author)
This manuscript has been revised thoroughly according to the provided comments, and it could be accepted for publication in Nature Communications.

Replies to the Reviewers' Comments

Thank you for your advice and guidance. We also would like to take this opportunity to thank the unnamed reviewers for their invaluable advice and suggestions on our work. We have revised the manuscript following the suggestions from the reviewers. Below are our response and answers to the reviewers' comments and questions on our manuscript (**NCOMMS-25-83721**). Our response to reviewer comments will be in blue color and the revised parts in red color, which are highlighted in yellow color in the revised Manuscript and Supplementary Information.

We hope that our responses to the comments and the revised manuscript will meet with approval.

Reviewer: #1

COMMENTS TO AUTHOR:

This manuscript describes the design and electrochemical investigation of a K^+-substituted high-entropy Prussian blue analogue (K-HEHCF) for enhanced capacitive deionization and energy recovery applications. The authors systematically analyze the structural stabilization effects induced by both high configurational entropy and K^+ substitution, demonstrating improved water resistance, lattice stability, and energy recovery efficiency compared to conventional HEHCFs. The manuscript is well organized, and the experimental data are comprehensive and clearly presented.

Response: We thank the reviewer for the valuable comments and suggestions. All the concerns raised from the reviewer have been addressed in detail as follows.

1. While the manuscript is well executed, the originality of the work is somewhat limited. The authors have previously reported a high-entropy PBA system in Advanced Science (2024) (Ref. 35), and the present study appears to be an extension of that concept through the incorporation of K^+ substitution. However, the effects of K^+ ions on PBA frameworks—such as water-content reduction, structural stabilization, and partial ion-exchange behavior—have already been well documented in the literature. In particular, K^+-substituted HE-PBAs have recently been reported in Desalination (617 (2026) 119487). Therefore, the distinct contribution of this study should be more clearly emphasized.

Response: We sincerely appreciate the reviewer's detailed comments on the innovative aspects of this work. We fully acknowledge that high entropy PBA materials and K substitution strategies have established research foundations in relevant fields.

However, this work is not merely an extension of K substitution based on our earlier HE-PBA design, but rather the first systematic coupling of the high entropy concept with precise K^+ regulation within the CDI field. It jointly reveals the synergistic enhancement mechanism between the two from multiple dimensions, including water content, ion diffusion kinetics, cycling stability, and capacitance contribution mechanisms. Simultaneously, it thoroughly explores the advantages of K substitution for Na and the storage mechanism of Na ions.

The unique and novel contributions of this work, compared with existing literature, are highlighted as follows:

First, unlike single high entropy strategies or isolated K^+ substitution, this work demonstrates for the first time the synergistic effect of high entropy configurations and K^+ substitution, simultaneously achieving low defect density, low water content, high stability, and high-rate capacitive behavior (*Angewandte Chemie Int. Ed* ***2023****, 62, e202303953*).

Second, it systematically elucidates the stabilization mechanism of K^+ regulation in high entropy PBA frameworks, clarifying its unique role in suppressing lattice collapse, reducing water content, enhancing ion transport, and facilitating reversible adsorption-desorption (*Desalination* ***2026****, 617, 119487*).

Third, most reported studies on high entropy PBAs have focused on a single cation system, with few comprehensive and systematic comparisons between K^+ and Na^+-based PBAs. Through this direct comparative experiment, our work clearly demonstrates that K^+ substitution is key to further enhancing the desalination performance of high entropy PBAs, constituting a significant innovation and highlight that distinguishes this research from existing literature.

Page 5, line 90 in manuscript, added: "Recent reports on high entropy PBAs research have mostly focused on a single cation system or remained limited to comparisons with low entropy PBAs, demonstrating improved CDI performance. However, comprehensive and systematic comparisons between K^+ and Na^+-based PBAs have been scarce."

2. The manuscript frequently attributes the superior performance of K-HEHCF to the synergistic effect between high configurational entropy and K^+ incorporation. However, this synergy has not been rigorously validated, as the two factors are not experimentally decoupled.

Response: Thank you for your professional comments. The outstanding performance of K-HEHCF stems from the combined effects of K substitution and configuration entropy. We supplemented the CV testing of Na-MnHCF and calculated its specific capacitance, revealing that K-MnHCF exhibits superior capacitive performance compared to Na-HEHCF (Supplementary Figs. 14 and 15). Furthermore, combined with the cyclability and water content tests of Na- and K-based PBAs supplemented in Comment 3, it can be observed that K substitution exerts a positive influence on the structure of HCFs. However, the limitations of single-metal-site persist. At this point, we introduce the concept of high entropy, incorporating multiple metallic elements into PBAs. Leveraging the inherent high stability of high configurational entropy and the "cocktail effect", we couple this with the low water content and low lattice defect advantages achieved through K substitution. This synergistic approach delivers a significant enhancement in the performance of K-HEHCF. As shown in Fig. R1, the CDI curves indicate that the MnHCF phase after K substitution exhibits reduced side reactions compared to Na-MnHCF, yet its adsorption capacity remains poor. In contrast, the CDI process for K-HEHCF becomes normalized with excellent adsorption capacity. Therefore, we conclude that the synergistic effect of K substitution and the high entropy effect collectively endows K-HEHCF with its outstanding performance.

Page 9, line 188 in manuscript, revised: "The CV plot of K-MnHCF at the same scan rate is similar, but the redox peaks are not symmetrical (Supplementary Fig. 14a). The specific capacitance of K-MnHCF is slightly higher than that of Na-MnHCF, which may result from reduced lattice defects in MnHCF due to K substitution for Na (Supplementary Fig. 15)."

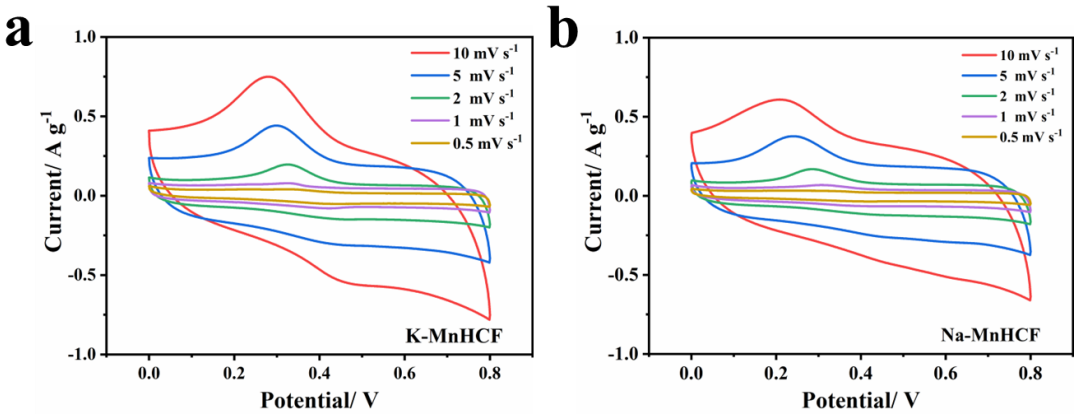

Supplementary Fig. 14 CV curves of (a) K-MnHCF and (b) Na-MnHCF at different scan rates.

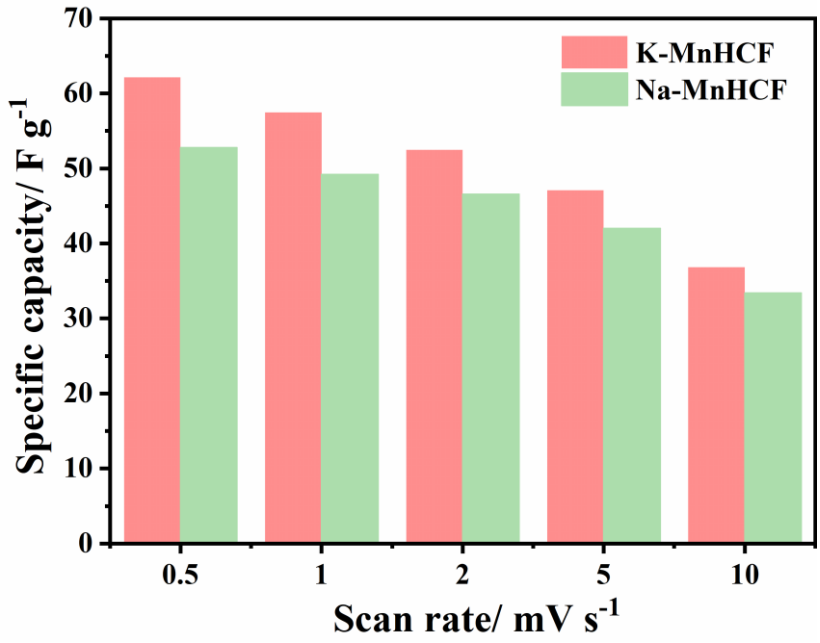

Supplementary Fig. 15 Comparison of Specific capacitance of (a) K-MnHCF and (b) Na-MnHCF.

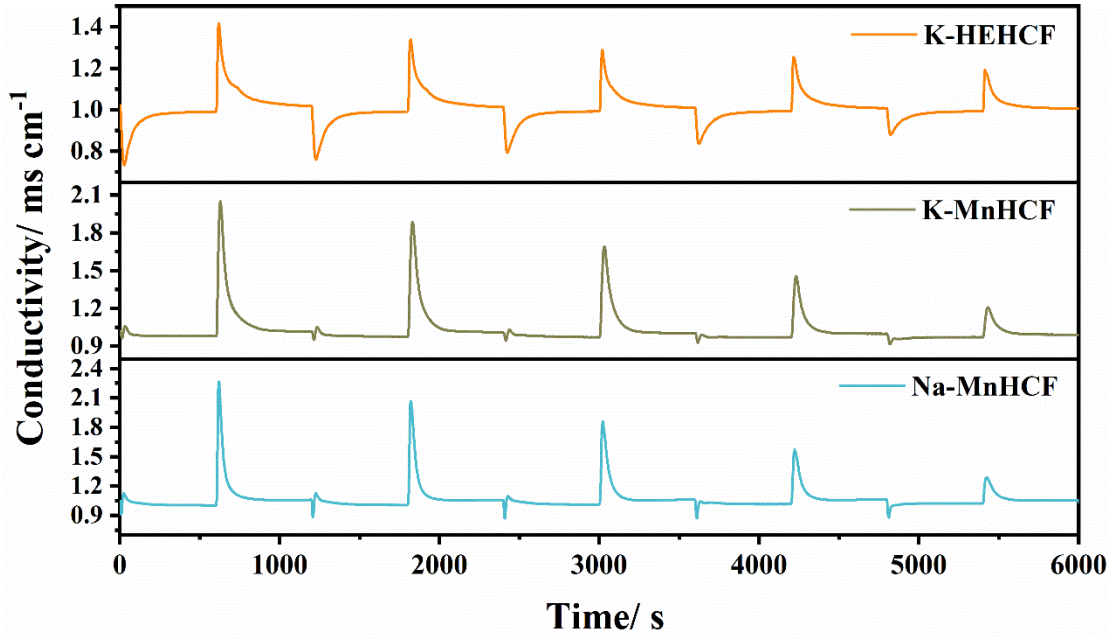

Fig. R1 CDI desalination curve for a NaCl solution with an initial concentration of 500 mg L^{-1}

3. To generalize the proposed mechanism, the authors are encouraged to compare the K^+ substitution behavior in other metal-centered PBAs (e.g., Co–HCF, Ni–HCF, or Fe–HCF). This would help clarify whether the observed "pillar effect" and water-content suppression are universal phenomena or specific to Mn-based systems.

Response: Many thanks for your insightful comments. Following the reviewer's suggestion, we synthesized HCFs with other single-metal-center elements besides Mn (Fe-HCF, Co-HCF, Ni-HCF, and Cu-HCF). The XRD patterns are shown in Supplementary Figs. 31a-c. The results indicate that K-based PBAs exhibited superior capacity retention ratio compared to Na-based PBAs after 100 CDI cycles (Supplementary Figs. 31d-f). Additionally, we measured the K:Na atom ratio in K-HEHCF after different cycling cycles (Table R1), further validating the claim that incomplete exchange of Na and K ions occurs during cycling. The residual K^+ ions within the lattice can exert a "pillar effect" to stabilize the framework structure (Fig. 5b-g).

Thermogravimetric analysis (TGA) reveals the water content of different HCFs, with interstitial water content of K-based Fe-HCF, Co-HCF, Ni-HCF, and Cu-HCF being 5.26%, 2.93%, 6.87%, and 6.24%, respectively; while the coordinated water content was 4.43%, 0.64%, 1.17%, and 4.63%, respectively. In contrast, the interstitial water contents of Na-based Fe-HCF, Co-HCF, Ni-HCF, and Cu-HCF were 8.99%, 6.04%, 9.55%, and 6.94%, respectively; the coordinated water contents were 12.12%, 7.35%, 7.89%, and 11.87% (Fig. 32). These results align with those for HEHCFs and MnHCFs, indicating that K substitution effectively suppresses the water content of PBAs and reduces defect formation regardless of whether the center is polymetallic or monometallic.

In summary, the observed "pillar effect" and water-content suppression are universal phenomena. These interact synergistically with the high entropy strategy to enhance K-HEHCF, resulting in outstanding performance. This strategy establishes a new paradigm for synthesizing structurally stable, low-defect electrode materials that simultaneously exhibit high sodium storage efficiency.

Page 15, line 316 in manuscript, added: "Furthermore, cyclic stability testing and TGA of other single-metal-center PBAs also indicate that the mechanism underlying the superior performance of K-based PBAs over Na-based PBAs is not limited to Mn-based materials. The K-HEHCF material, synthesized by further coupling K substitution MnHCF with a high entropy strategy, exhibits outstanding electrochemical and desalination performance. This strategy provides a novel approach and design paradigm for constructing electrode materials with stable structures, low lattice defects, and high sodium-ion storage efficiency (Supplementary Figs. 31-32)."

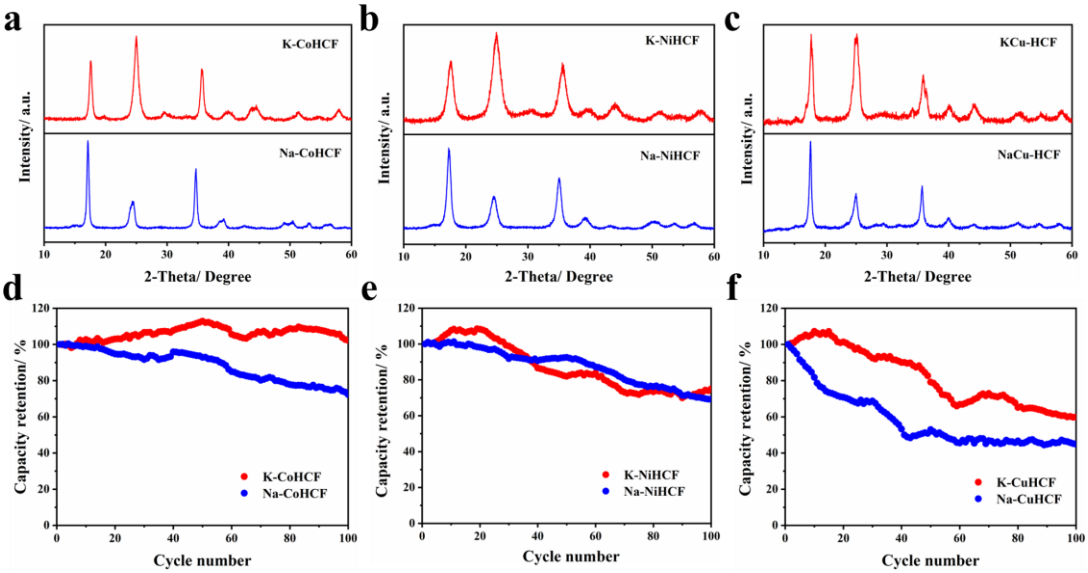

Supplementary Fig. 31 XRD patterns and capacity retention of other single metal-centered PBAs at 1 V.

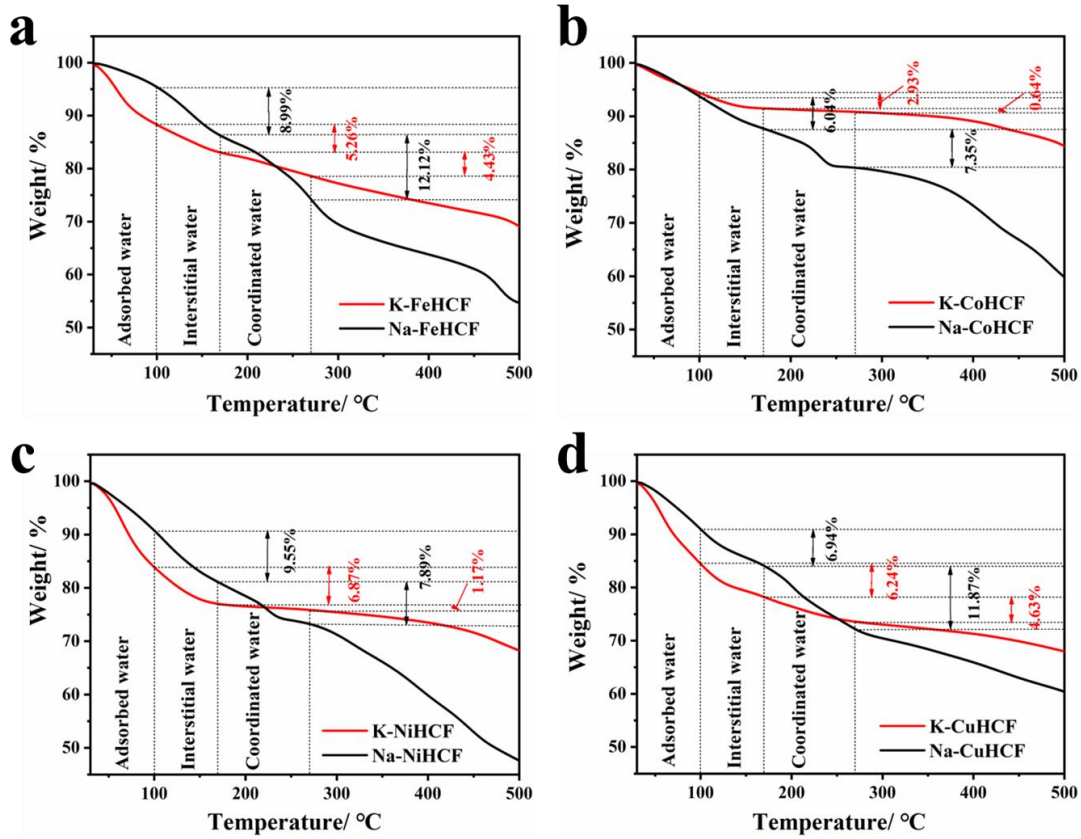

Supplementary Fig. 32 TGA curves of (a) FeHCFs, (b) CoHCFs, (c) NiHCFs and (d) CuHCFs.

Table R1. Atomic ratios of different elements in K-HEHCF after different cycles determined by XPS analysis.

Sample	Cycles	K/ at.%	Na/ at.%
K-HEHCF	0	11.31	0
	50	0.29	1.28
	100	0.32	1.09
	200	0.2	1.3

4. The CDI performance is impressive, but additional quantitative metrics are necessary to assess the practical feasibility of the proposed system. Specifically, the following data are recommended:

- Energy consumption per mole of salt removed (kWh mol^{-1} or kWh m^{-3}).
- Long-term electrode lifetime and structural stability beyond 200 cycles.
- Coulombic efficiency and true energy recovery ratio during charge/discharge cycles.

Response: Thank you very much for your pertinent comment. CDI performance stands as one of the most critical highlights in our work. Below, we provide a point-by-point explanation and supplement regarding the aspects raised in the comments.

First, we recalculated the molar energy consumption of K-HEHCF and Na-HEHCF at different voltages, with results shown in Supplementary Fig. 30. The energy consumed by K-HEHCF samples during CDI was significantly lower than that of Na-HEHCF, particularly at the selected optimal voltage of 1.4 V. This low energy consumption is more conducive to practical applications, as mentioned in our article, the K substitution strategy significantly enhances the desalination capacity of HEHCF.

Second, the long-term cycling performance of electrode materials is undeniably crucial for the practical application of CDI. Therefore, we conducted CDI cycling tests on K-HEHCF for up to 200 cycles. The results demonstrated that the cycle retention rate remained above 95%, fully validating the importance of high configurational entropy in suppressing unfavorable phase transitions during the reaction process. Furthermore, we compared the CDI performance of K-HEHCF with that of the recently reported Faraday electrode material. It is evident that K-HEHCF significantly outperforms in terms of adsorption capacity and cycle life, clearly demonstrating its

excellent CDI performance and practical application potential. This sufficiently supports the core conclusions of this work. We will also conduct longer-cycle testing in future applied research (Fig. 4g and Supplementary Table 11).

Third, we calculated the coulombic efficiency and true energy recovery rate of K-HEHCF during CDI cycles. As shown in the figure, the decline in coulombic efficiency during the early cycling stage may be attributed to irreversible losses during electrode surface activation and increased hydrophilicity(*Advanced Materials* ***2023****, 35, 2210871; Journal of Materials Chemistry A* ***2015****, 3, 23864*). This process also corresponds to the enhanced desalination capacity of K-HEHCF in the early cycling phase (Figure 4f). As cycling progresses, the electrode system gradually achieves a stable adsorption-desorption equilibrium, with the coulombic efficiency stabilizing and maintaining above 90%, indicating excellent reversibility and structural stability of the electrode. Since the charge-discharge voltage during cycling is ±1 V, the calculated true energy recovery rate aligns with the coulombic efficiency (Supplementary Fig. 34).

Page 16, line 331 in manuscript, added: "As cycling progresses, the electrode system gradually achieves a stable adsorption-desorption equilibrium, with the coulombic efficiency stabilizing and maintaining above 90%, indicating excellent reversibility and structural stability of the electrode. Since the charge-discharge voltage during cycling is ±1 V, the calculated true energy recovery rate aligns with the coulombic efficiency (Supplementary Fig. 34)."

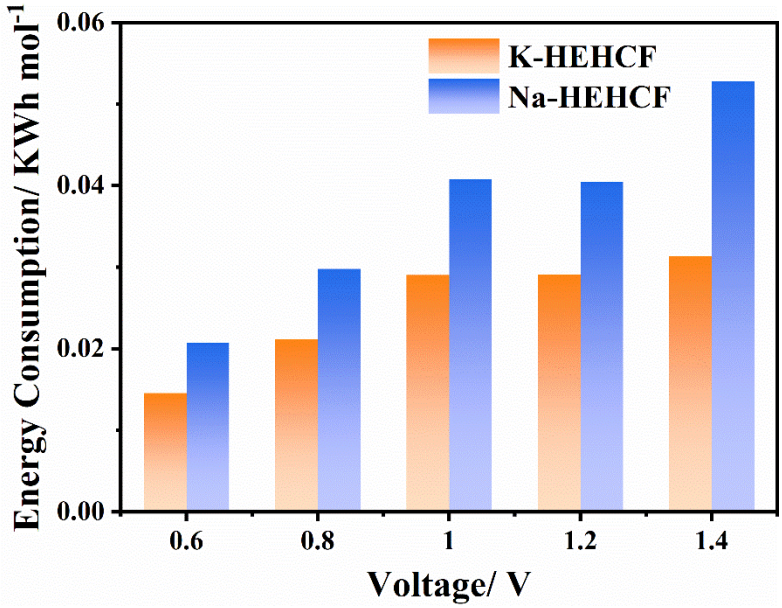

Supplementary Fig. 30 The energy consumption of K-HEHCF and Na-HEHCF at various voltage with 500 mg L^{-1} NaCl solution.

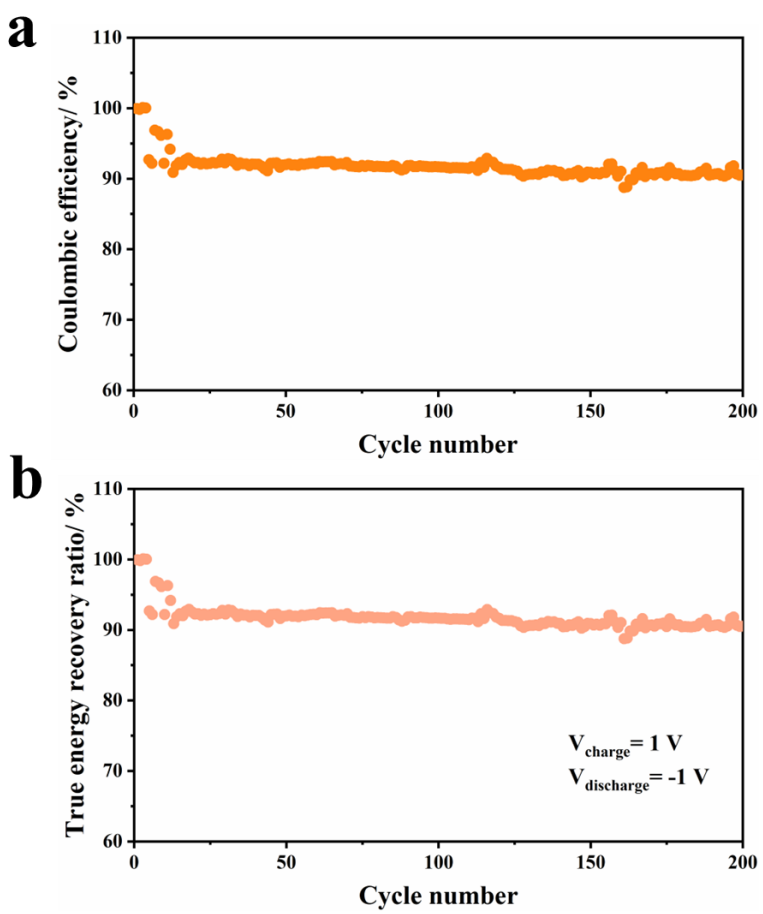

Supplementary Fig. 34 (a) Coulombic efficiency and (b) true energy recovery ratio during CDI cycles.

Reviewer: #2

COMMENTS TO AUTHOR:

In this manuscript, K-based high entropy hexacyanoferrate (K-HEHCF) is successfully synthesized by a one-step co-precipitation method. This electrode material can achieve good electrical conductivity and stability. The successful synthesis of the electrode material was demonstrated by various characterizations, and good desalination performance can be achieved in CDI applications. However, the experimental content of this manuscript is not novel enough, the materials are not innovative, so it cannot be accepted. The following are rejection reasons.

Response: We thank the reviewer for the valuable comments and suggestions. All the concerns raised from the reviewer have been addressed in detail as follows.

1. Please give the contents of different elements in K-HEHCF and Na-HEHCF to prove the mole fractions of the five elements are close to each other with about 0.2 using ICP and calculate the configuration entropy to ensure that ΔSconf > 1.5R.

Response: Thank you very much for your comments. The ICP-OES test results for K-HEHCF and Na-HEHCF are shown in Supplementary Table 1.

Supplementary Table 1 ICP-OES results of element ratios for K-HEHCF and Na-HEHCF.

Element	K	Fe	Mn	Co	Ni	Cu
Mole ratios	2.07	0.94	0.21	0.2	0.22	0.2

Element	Na	Fe	Mn	Co	Ni	Cu
Mole ratios	3.02	0.75	0.24	0.22	0.18	0.19

Calculate the configuration entropy of K-HEHCF and Na-HEHCF according to equations 1-2 of the Methods.

$$\Delta S_{\mathrm{conf}} = -R\sum_{i=1}^{n} x_i \ln x_i \qquad (1)$$

$$\Delta S_{\mathrm{K-HEHCF}} = -R(0.17\ln 0.17 + 0.21\ln 0.21 + 0.2\ln 0.2 + 0.22\ln 0.22 + 0.2\ln 0.2) = 1.61R$$

$$\Delta S_{\mathrm{Na-HEHCF}} = -R(0.17\ln 0.17 + 0.24\ln 0.24 + 0.22\ln 0.22 + 0.18\ln 0.18 + 0.19\ln 0.19) = 1.60R$$

$\Delta S_{\mathrm{K-HEHCF}} > 1.5\mathrm{R}$, $\Delta S_{\mathrm{Na-HEHCF}} > 1.5\mathrm{R}$.

The computational results indicate that the configuration entropies of both K-HEHCF and Na-HEHCF exceed 1.5 R, placing them within the high entropy category. **Page 6, line 119 in manuscript**, revised: "ICP-OES results indicate that the main transition metal elements in K-HEHCF are Fe, Mn, Co, Ni, and Cu, and the mole fractions of the five elements are close to each other with about 0.2. The ΔS_{conf} can be determined using the definitions derived from statistical thermodynamics, based on the Eqs. 1-2, we can calculate the ΔS_{conf} of K-HEHCF as 1.61R, which exceeds 1.5R and reaches high entropy category (Supplementary Table 1)."

2. The pseudo-capacitance calculation results of electrochemical tests show that the capacitance contribution rate of K-HEHCF increases from 34.4% to 81.6%. Why does this part of the data show that the proportion of capacitance is relatively small? Please explain and modify it. Please re-select the small sweep speed range and calculate the capacitance contribution more convincingly.

Response: Thank you for your comments. During CV testing in the manuscript, I employed scanning rates ranging from 0.5 to 10 mV s^{-1}. Using these CV curves, I calculated the capacitive contribution via Dunn's method, which increased from 34.4% at 0.5 mV s^{-1} to 81.6% at 10 mV s^{-1}. However, as you mentioned, the early capacitive contribution calculated at higher scan rates is relatively low, ions struggle to diffuse sufficiently into the active sites within the material in a short time, leading to diffusion-controlled processes dominating the reaction. To obtain a more reliable contribution ratio for the dynamics, calculations were re-performed within the low scan rate range of 0.2-1.0 mV s^{-1}, the percentage contribution from capacitance increased from 67.8% at 0.2 mV s^{-1} to 82.1% at 1 mV s^{-1} (Fig. 3e and Supplementary Fig. 19). At low scan rates, ion diffusion and charge transfer processes become more thorough, significantly enhancing the proportion of capacitive control and improving its authenticity. The rapid charge-discharge capability of K-HEHCF electrodes facilitates efficient and stable capacitive deionization behavior.

Page 11, line 216 in manuscript, revised: "To obtain a more reliable kinetic contribution ratio, we performed calculations using a low scanning rate range of 0.2-1.0 mV s^{-1}. After calculation, the b values of the two peak currents of K-HEHCF are 0.95 and 0.94 respectively (Supplementary Fig. 18)."

Page 11, line 220 in manuscript, revised: "It can be observed that the capacitive contribution increases with the increase in scan rate, from 67.8% at 0.2 mV s^{-1} to 82.1%

at 1 mV s^{-1} (Fig. 3e and Supplementary Fig. 19), indicating that the ion/charge migration is mainly controlled by capacitive control."

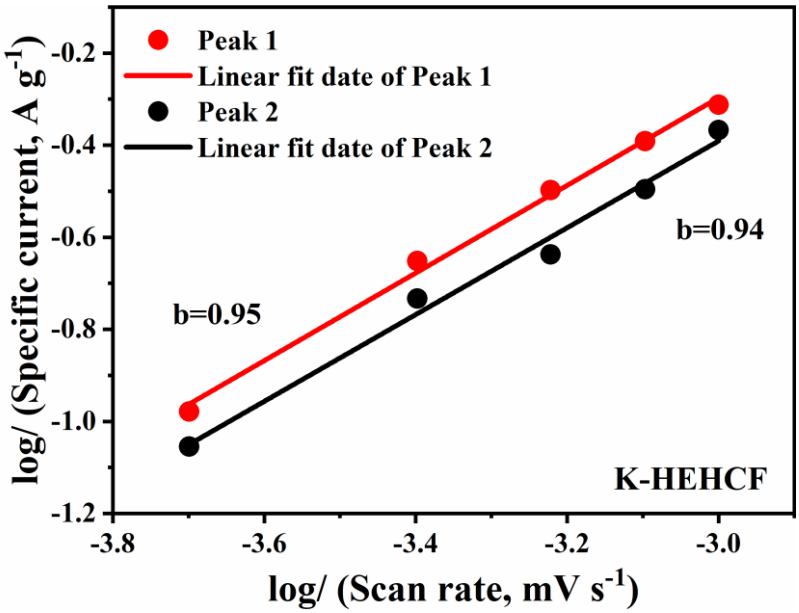

Supplementary Fig. 18 Linear correlation between the logarithmic peak current and sweep rate of K-HEHCF.

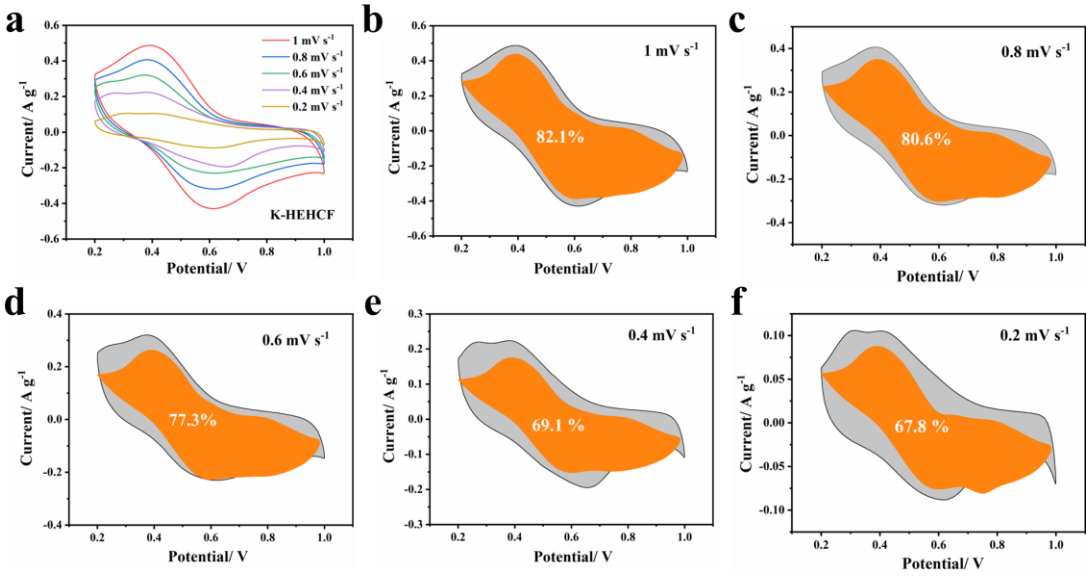

Supplementary Fig. 19 The contribution of capacitive-controlled (color) and diffusion-controlled process (grey) of K-HEHCF at different scan rates.

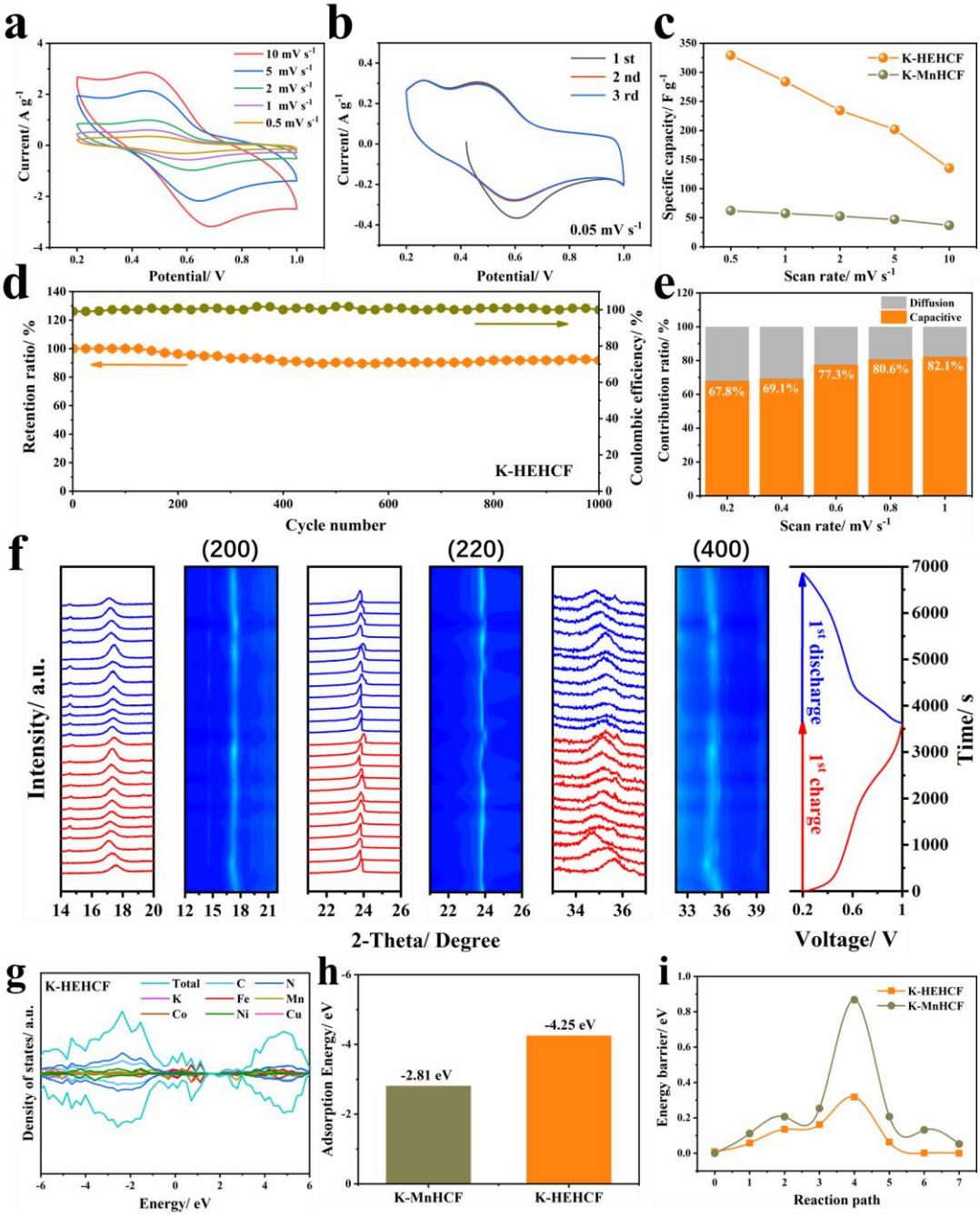

Fig. 3: Electrochemical properties and ion-capture mechanism of K-HEHCF. a CV curves of K-HEHCF at different scan rates. **b** CV curves for the first three cycles at a scan rate of 0.05 mV s^{-1}. **c** Comparison of Specific capacitance. **d** Cycling performance and coulombic efficiency at 2 A g^{-1} for 1000 GCD cycles. **e** The capacitive-controlled and diffusion-controlled contribution percentage of K-HEHCF. **f** Ex situ XRD patterns of K-HEHCF during the first cycle and corresponding charge/discharge curves. **g** Density of states of **a** K-HEHCF. **h** Calculation of the adsorption energy of Na on the HCFs surface. **i** The corresponding migration barrier energies for paths in different HCFs.

3. Why the K-HEHCF have good removal efficiency for the common multivalent salt ions, especially for Ca^{2+}?

Response: Thanks for your invaluable suggestions. As you can see, we designed a multi-channel tandem CDI system with five treatment units (Figure S33) to treat simulated circulating cooling water. The coupled CDI system exhibited excellent mixed-ion separation performance in the simulated circulating cooling water. The Ca and Mg ions in the treated simulated circulating cooling water were almost negligible, especially for Ca^{2+}.

This is mainly due to the following reasons:

First, the application of CDI technology for the selective extraction of different ions from saltwater has been reported for some time, and He et al. (*Environmental Science & Technology* ***2018****, 52, 9350-9360; Separation and Purification Technology* ***2022****, 280, 119828; Advanced Functional Materials* ***2021****, 31, 2105203*) have achieved the selective removal of divalent Ca^{2+} and Mg^{2+} cations compared with monovalent Na^{+} by optimizing the operating conditions in the face of high hardness brackish water, which provides us with theoretical support.

Second, there are specific ion exchange sites in the crystal structure of Prussian blue analogs, and the size, shape and charge distribution of these sites are selective for the exchange of different ions. The size and charge distribution of multivalent ions may be better suited for these exchange sites, for example, Zhao et al. (*Journal of Colloid and Interface Science,* ***2012****, 384, 38-44*) reported that in a typical capacitive deionization device, monovalent Na^{+} ions are initially adsorbed when a voltage difference is applied between the two electrodes, and are subsequently gradually replaced by divalent Ca^{2+} ions at lower concentrations. Therefore, after complete adsorption, K-HEHCF exhibits a preference for divalent ions in mixed ionic solutions, achieving highly efficient removal of Ca^{2+} and Mg^{2+}. In addition, from the energy point of view, the binding energy of multivalent ions with K-HEHCF is usually higher than that of Na^{+}. This means that the conjugates formed by Ca^{2+} and Mg^{2+} with K-HEHCF are more stable, and once Ca^{2+} and Mg^{2+} come into contact with and bind to K-HEHCF, they are not easy to be detached from the structure again, resulting in a higher selectivity and efficiency of Ca^{2+} and Mg^{2+} removal by K-HEHCF.

Third, from the perspective of diffusion speed, in general, the higher the charge density of an ion, the relatively slower its diffusion speed in solution. Since Na^{+} has a lower charge density and a smaller hydration radius, its diffusion speed in solution is

relatively faster, but this also makes its bonding with the surface of K-HEHCF relatively unstable, and it is easy to be detached again in the diffusion process. On the other hand, Ca^{2+} and Mg^{2+} have relatively slower diffusion speeds due to their higher charge density and larger hydration radius, but once they come into contact with the K-HEHCF surface, they are more inclined to be exchanged with and immobilized in the structure of K-HEHCF due to stronger electrostatic interactions, which improves the removal efficiency.

In summary, the removal efficiency of K-HEHCF for Ca^{2+} and Mg^{2+} ultimately exceeds that for Na^{+}, a result influenced by the combined effects of ion exchange thermodynamics, kinetics, and ion hydration radius.

Page 16, line 326 in manuscript, added: "In fact, numerous research studies have already investigated the feasibility of selectively extracting different ions from saltwater using CDI technology. Meanwhile, Prussian blue analogues such as K-HEHCF possess specific ion exchange sites within their crystal structures. The size, shape, and charge distribution of these sites confer selectivity toward different ions, with multivalent ions potentially exhibiting a more suitable size and charge distribution for these exchange sites. During adsorption, Na^{+} with lower charge density and smaller hydration radius typically adsorb preferentially due to their faster diffusion rate, but their binding is unstable. As adsorption approaches saturation, Ca^{2+} and Mg^{2+} with higher charge density and larger hydration radius are more readily attracted and fixed by the high charge density regions on the K-HEHCF surface. At this point, Na^{+} is often at a disadvantage in the adsorption competition and is eventually replaced by Ca^{2+} and Mg^{2+}. Consequently, K-HEHCF demonstrates excellent removal efficiency for Ca^{2+} and Mg^{2+}."

4. Please compare the contents of K and Na in materials before and after cycling to prove the exchange of K and Na during the reaction process. "Part of K^{+} will stay in K-HEHCF to be the backbone". Will this part K^{+} gradually decrease during long-term cycling, or will it remain in the material during long-term cycling? Please confirm it.

Response: Many thanks for your insightful comments about our manuscript. Upon initial analysis, we compared only the K^{+} content in K-HEHCF before and after the cycle to demonstrate that a small amount of K^{+} consistently remains throughout the process, exerting a "pillar effect". As requested by the reviewer, we have supplemented the data with the Na^{+} content changes in K-HEHCF during this process to confirm the

exchange of K and Na during the reaction (Supplementary Fig. 38). During the cycling process, the intensity of the K 2p characteristic peak from strong to weak, while the intensity of the Na 1s characteristic peak from absent to present, precisely confirming the exchange behavior between Na and K during this period.

We attempted to further confirm the Na^+/K^+ exchange of K-HEHCF during the charge-discharge process by 2D mapping spectra of TOF-SIMS. As seen in Figs. 5e-g, Na^+ was not present in the maps of the initial sample. However, from the maps of the sample after ten times of charging, it can be found that the Na^+ signals are obviously strengthened and the K^+ signals are weakened, indicating that Na^+ replaces part of the K^+ in the lattice, and the replaced K^+ is dissolved into the electrolyte. The sample maps after the subsequent discharge shows a reversible recovery of K^+, but not back to the initial strength, while the Na^+ signal strength continues to be strengthened. This may be due to the fact that the concentration of free Na^+ in the electrolyte is much higher than that of K^+, and the radius of Na^+ is smaller than that of K^+. In summary, K^+ and Na^+ undergo ion exchange during the reaction process, and the remaining K^+ is believed to be the backbone for reducing structural strain and stabilizing the framework, and may lead to long-term cycling performance.

Additionally, XPS analysis of K-HEHCF after different cycling cycles revealed a rapid decrease in K^+ content following reaction initiation, ultimately stabilizing at 0.2–0.3%. This process was accompanied by an increase and stabilization of Na^+, indirectly demonstrating that residual K^+ from the reaction remains stably present within K-HEHCF during long-term cycling and continues to exert its function (Table R1).

Page 17, line 351 in manuscript, revised: "As illustrated in Fig. 5b, the line-scan spectra of the K-HEHCF electrodes after CDI cycling showed significant K and Na signals, while the EDS spectra of K 2p also indirectly confirmed the residual of trace K^+ (Supplementary Fig. 37). Analysis of the evolution of high-resolution K 2p and Na 1s spectra before and after the K-HEHCF cycle further verifies the occurrence of reversible ion exchange between K^+ and Na^+(Supplementary Fig. 38)."

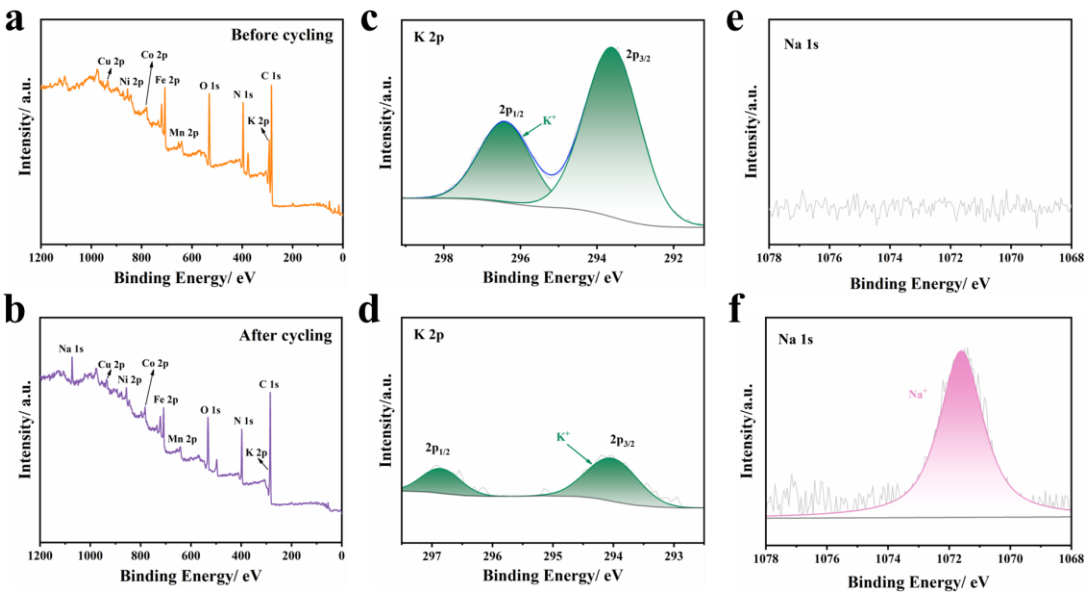

Supplementary Fig. 38 (a, b) XPS survey spectra, (c, d) K 2p and (e, f) Na 1s spectra of K-HEHCF before and after cycling.

Table R1. Atomic ratios of different elements in K-HEHCF after different cycles determined by XPS analysis.

Sample	Cycles	K/ at.%	Na/ at.%
K-HEHCF	0	11.31	0
	50	0.29	1.28
	100	0.32	1.09
	200	0.2	1.3

5. There are several similar published papers like https://doi.org/10.1021/acsnano.3c02323; https://doi.org/10.1007/s12274-022-5020-0; https://advanced.onlinelibrary.wiley.com/doi/10.1002/adfm.202510533.

Response: We thank the reviewer for the valuable comments and suggestions. The three works you mentioned are all outstanding and provide invaluable guidance for our subsequent research. Currently, the integration of the high entropy concept with Prussian blue has garnered increasing attention across various fields. This study differs from these previous works in the following aspects:

First, the aforementioned literature focuses on capacity, voltage optimization, and catalytic efficiency of energy storage batteries (Na-ion/ Zn-ion/ Li-CO_2 batteries). This work, however, targets enhancing the desalination performance of CDI, addressing the core challenge of achieving a balance between kinetics and high desalination capacity in CDI electrodes (*Coordination Chemistry Reviews* ***2024****, 520, 216100*).

Second, this work extends high entropy strategies and precise cation regulation to the CDI context, revealing their synergistic mechanism in enhancing desalination reversibility and kinetic performance. It establishes a new paradigm for cation design in CDI electrodes, distinct from the battery material optimization logic described in the aforementioned literature.

Third, the literature mentioned by the reviewer demonstrates performance optimization through a simple comparison between high entropy PBA and low or medium entropy PBAs, revealing a somewhat limited research perspective. In fact, as early as 2024, we proposed the core concept, reporting a high entropy Prussian blue analogue (HE-PBA) and systematically revealing the enhancement mechanism of high configurational entropy on the electrochemical performance of materials (*Advanced Science* ***2024****, 11, 2402340*). In this study, we did not confine ourselves to a single entropy engineering strategy. Instead, we achieved a critical expansion and performance upgrade of this concept through the innovative coupling of high entropy structures with K^+ substitution. Distinct from prior work, we conducted systematic comparative experiments between K^+- and Na^+-based PBAs across multiple core dimensions: crystalline water content, cycling stability, capacitive contribution mechanisms, and ion diffusion kinetics. This not only unequivocally demonstrated K ions significant structural and performance advantages but also elucidated its unique role in reducing lattice water content, enhancing ion adsorption capacity, suppressing structural distortion, and improving cycling reversibility. This provides a more comprehensive and targeted design approach for optimizing the performance of PBA-based electrode materials.

6. What is the mass of K-HEPBA and AC electrode respectively? In the desalination test, an area of 4.5*6.5 cm^2 is used, and the desalination performance test is greatly affected by the mass and area of the electrode, so please fully compare the desalination capacity of HEPBA with different mass and area.

Response: Thanks for the professional suggestion. The K-HEHCF and AC electrodes used in the CDI experiment weighed 32 – 36 mg each. They were fabricated by casting

a slurry mixture of active materials (AC, PBAs), carbon black, PVB, and PVP in a mass ratio of 8:1:1 onto graphite paper.

As the reviewer noted, desalination performance tests are significantly influenced by electrode mass and area. Therefore, to fully validate the optimal desalination performance of HEHCFs, we prepared three additional CDI electrodes with varying mass or area: 4.5×6.5 cm^2 graphite paper electrode with a mass ratio of 24:3:3, 4.5×6.5 cm^2 graphite paper electrode with a mass ratio of 40:5:5, and 5.5×7.5 cm^2 graphite paper electrode with a mass ratio of 32:4:4 (Fig. R1).

The results are shown in the Supplement Fig. 29. In a 500 mg/L NaCl solution, the same electrode exhibited differences in adsorption capacity depending on its mass and area. Among the combinations tested, the 32:4:4 ratio with a 4.5×6.5 cm^2 electrode used in the manuscript demonstrated the best performance.

Page 15, line 310 in manuscript, added: "It is worth noting that since desalination performance testing is significantly influenced by electrode mass and area, we additionally prepared three CDI electrodes with different masses or areas and tested them to fully validate the optimal desalination conditions for K-HEHCF. The results indicate that the electrode conditions employed in this experiment exhibit optimal desalination performance (Supplementary Fig. 29)."

Page 26, line 533 in manuscript, revised: "Subsequently, the resulting slurry of solids (32:4:4 mg) was cast on a graphite paper (4.5×6.5 cm^2) and then dried at 80 ℃ overnight."

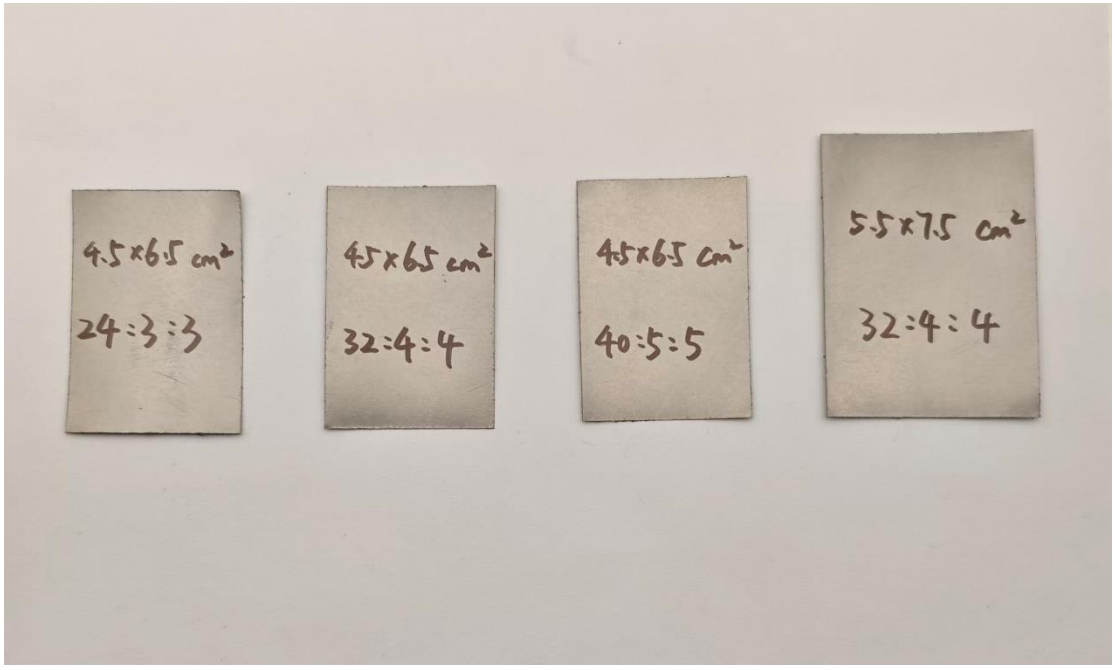

Fig. R1 Schematic diagram of CDI electrodes with different masses and areas.

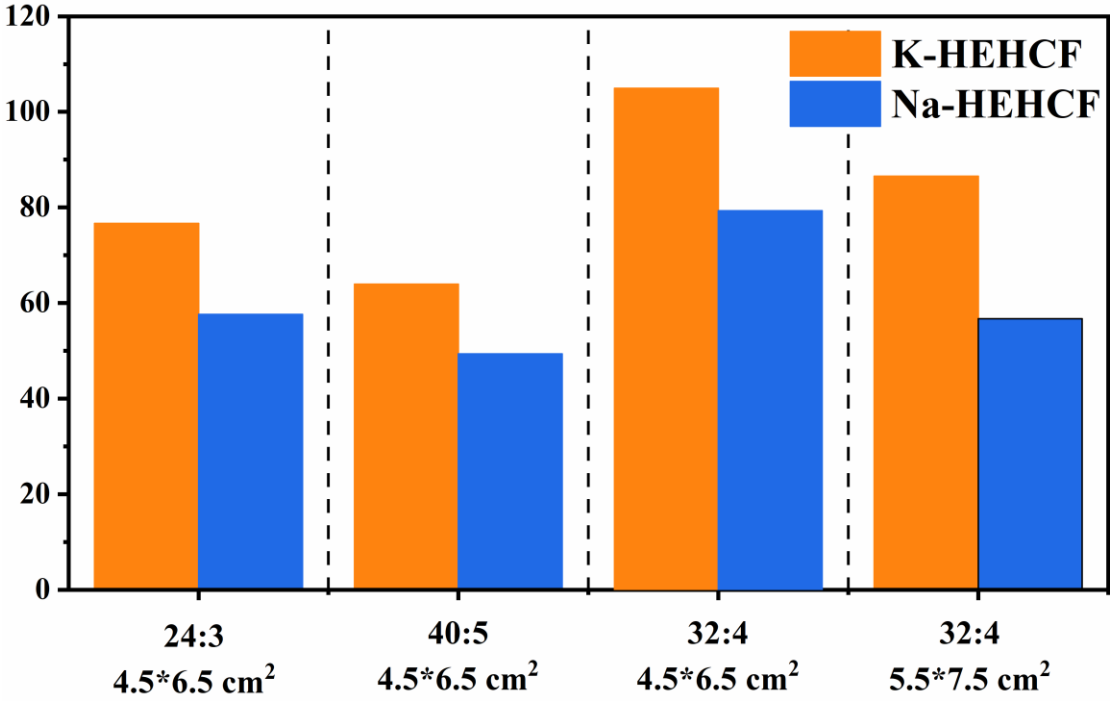

Supplementary Fig. 29 The adsorption capacity of K-HEHCF and Na-HEHCF at various conditions with 500 mg L^{-1} NaCl solution.

Replies to the Reviewers' Comments

On behalf of my co-authors, we thank you very much for giving us an opportunity to revise our manuscript. We would also like to once again thank the anonymous reviewers for their valuable suggestions and feedback on our research. We have revised the manuscript following the suggestions from the reviewers. Below are our response and answers to the reviewers' comments and questions on our manuscript (**NCOMMS-25-83721A**). Our response to reviewer comments will be in blue color and the revised parts in red color, which are highlighted in yellow color in the revised Manuscript and Supplementary Information.

We hope that our responses to the comments and the revised manuscript will meet with approval.

Reviewer: #1

COMMENTS TO AUTHOR:

The manuscript has been revised satisfactorily in accordance with the comments. It may be accepted for publication in Nature Communications.

Response: I would like to express my sincere gratitude for the many insightful professional comments and constructive suggestions you have provided. Your thoughtful feedback has greatly enhanced the quality of our paper, and we sincerely appreciate the effort and dedication you have shown throughout the review process.

Reviewer: #2

COMMENTS TO AUTHOR:

Although the authors have addressed several previous comments, there remain significant concerns regarding the electrochemical characterization and computational analysis sections. These issues are fundamental and must be resolved before the manuscript can be considered for publication. The main reasons for rejection are outlined below:

Response: We thank the reviewer for the valuable comments and suggestions again. Those comments are all valuable and very helpful for revising and improving our paper. All the concerns raised from the reviewer have been addressed in detail as follows.

1. According to the Methods section, the cyclic voltammetry (CV) measurements were conducted using a three-electrode system in 1 M NaCl, with scans performed from low to high voltage. However, in Figures 3a and 3b, the positions of the oxidation and reduction peaks are reversed compared with those reported in previous publications on HEPBA and PBA materials. Please clarify and explain this discrepancy. Furthermore, in Figure 3f, the galvanostatic charge–discharge (GCD) curve shows the oxidation peak as higher than the reduction peak, which is inconsistent with the CV profiles. please provide a clear explanation of this inconsistency and verify the accuracy of electrochemical data.

Response: Thank you very much for your careful review of the electrochemical characterization section of this research paper and for your constructive feedback. Below, I will provide detailed clarifications and explanations regarding the issues you raised.

First, compared to previous reports on HEPBA and PBA materials, the differences in the positions of the redox peaks shown in Figs. 3a and 3b are due to variations in the experimental setup of the electrochemical workstation. As described in the experimental section, the electrochemical measurements were conducted using a three-electrode system with a CHI 760E electrochemical workstation (Shanghai CH Instruments Co., China) in a 1 M NaCl solution. The experimental parameters are shown in Fig. R1a, with the current polarity set to cathode positive. Under these conditions, the CV results shown in the manuscript can be obtained (Fig. R1b). When the current polarity is set to anodic positive, the same CV test is performed on K-HEHCF, and the resulting plots are illustrated in Figs. R1c – d. Although differences in

the configuration of the chemical workstation may result in variations in the visual order of the redox peaks, this does not alter the redox nature of the material itself. The CV curves exhibit excellent reproducibility in terms of peak current and shape characteristics, thereby confirming the reversible Na^+ insertion/extraction process in K-HEHCF.

Second, the GCD curve in Fig. 3f shows that the oxidation plateau is higher than the reduction plateau, but the CV curve exhibits a symmetrical redox peak. This is due to the asymmetry in polarization and ion diffusion. During the charging process (oxidation reaction), the material undergoes slight structural contraction and exhibits relatively low polarization, resulting in the formation of a stable high-potential plateau. During the discharge process (reduction reaction), the material undergoes structural expansion, accompanied by slight kinetic hindrance, causing the working potential to decrease slightly, which makes the reduction plateau appear lower than the oxidation plateau. This kinetic asymmetry during charging and discharging is common and does not contradict the reversible redox peaks observed in the CV curve (*Chemical Science, **2024**, 15, 11814-11824; PNAS, **2026**, 123, e2525797123; Angewandte Chemie Int. Ed, **2025**, 64, e202501797*). The same GCD test was performed on three parallel samples of K-HEHCF at a current density of 1 A g^{-1}, as seen in the Fig. R2. It can be observed that, although there are slight differences in the charge and discharge times due to variations in the active mass of the electrodes, the shape of the curves remains unchanged, with the oxidation plateau being slightly higher than the reduction plateau, consistent with the results reported in the manuscript. Furthermore, the midpoint potential of the voltage plateau in the GCD curve corresponds to the average potential of the oxidation and reduction peaks in the CV curve, confirming that the redox potentials reflected by the two testing techniques are identical.

In summary, the observed differences are attributable to the current polarity settings and the kinetic asymmetry during the charging and discharging processes, rather than experimental errors or data inconsistencies. All electrochemical test results are reliable and chemically sound.

Page 9, line 183 in manuscript, revised: "The cyclic voltammetry curves of K-HEHCF are depicted in Fig. 3a, which exhibits a pair of distinct redox peaks in the 0.4-0.8 V range, which corresponded to the intercalation and deintercalation of Na^+ in the electrode, respectively."

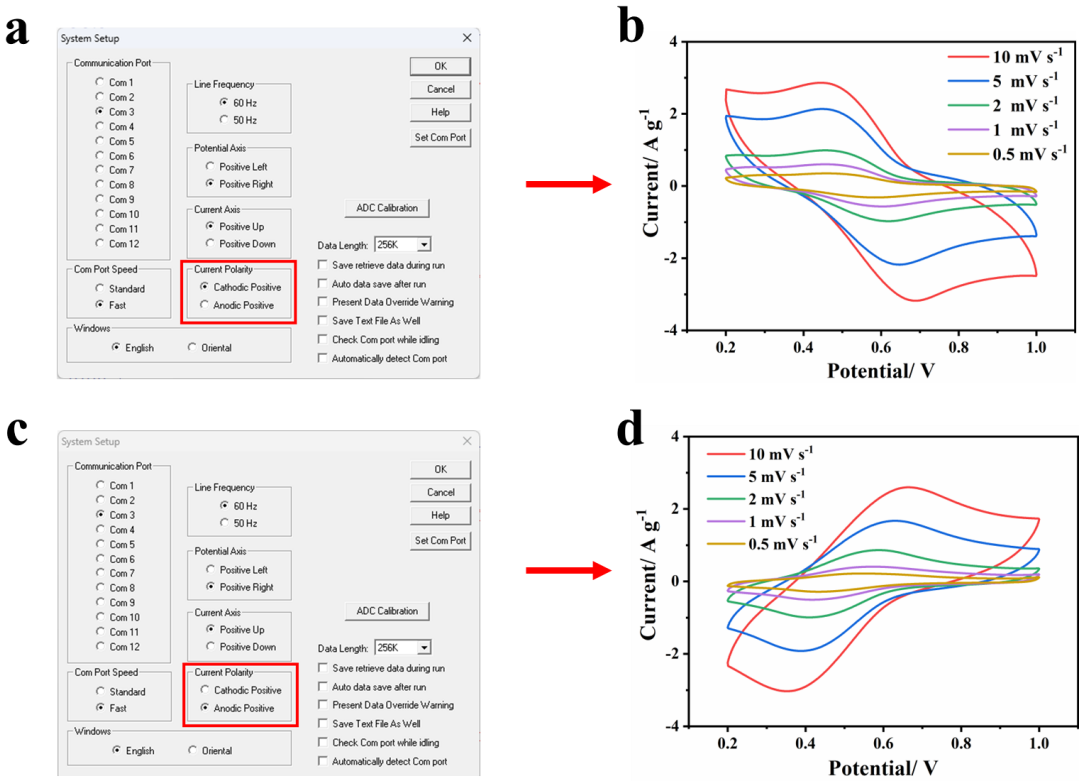

Fig. R1 (a, b) The experimental setup used in the manuscript and the resulting CV curves. (c, d) The modified experimental setup and the resulting CV curve.

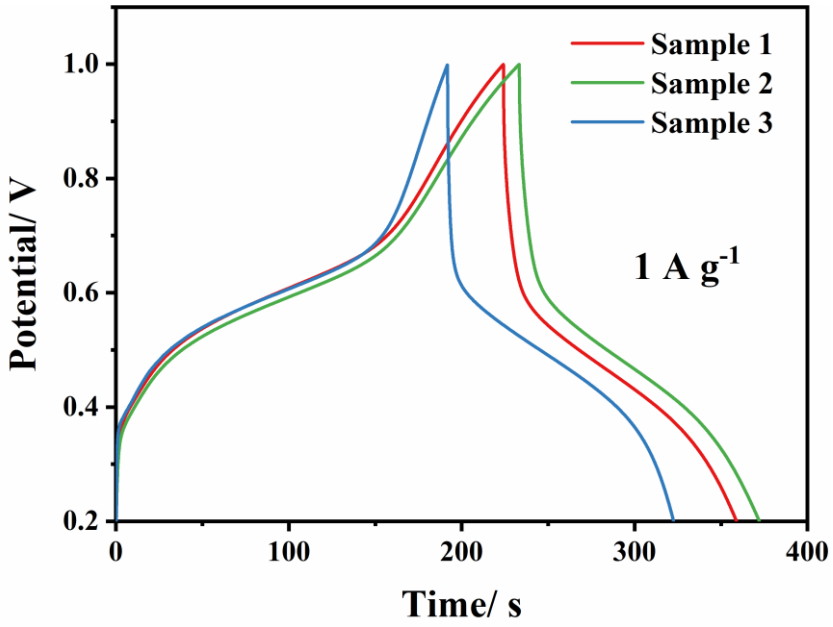

Fig. R2 GCD curves of K-HEHCF parallel samples at 1 A g^{-1}.

2. The manuscript lacks a dedicated Methods section describing the density functional theory (DFT) calculations. To ensure reproducibility and technical reliability, please add detailed information on the computational approach used. In addition, the raw

computational input files and key output files should be provided for all critical points and transition states discussed in the text.

Response: Thank you for your comments. A description of the density functional theory (DFT) computational method has been added to the Methods section. In addition, we have uploaded the raw computational files and key output files as Related Manuscript file under the filename "DFT DATA".

Page 26, line 529 in manuscript, added: "The computational analysis was carried out based on density functional theory (DFT) calculations, as implemented in Vienna ab initio simulation packages (VASP). The projector augmented wave (PAW) scheme and Perdew-Burke-Ernzerhof functional was used for geometric optimizations. In the geometric optimization, all atoms were allowed to relax until the calculated Hellmann-Feynman forces smaller than 0.03 eV/Å. The kinetic energy cutoff of 520 eV was chosen for the plane wave expansion."

3. For the adsorption energy study shown in Figure 5h, the optimized adsorption structure of Na-PBA should be provided. Regarding Figure 5i, the current number of images used is insufficient to accurately fit the reaction pathway, particularly for the green line. The authors should recompute the results using an adequate number of intermediate states and include the corresponding energy barrier values along with fully optimized atomic structures for the initial, intermediate, and final configurations.

Response: Thanks for your invaluable suggestions. We provide the optimized adsorption structures of K-HEHCF and K-MnHCF in the file and have inserted them as illustrations in Fig. 3h. In addition, we have provided further details regarding the NEB transition state calculations for the ion migration process of the green line (K-MnHCF), and have included the complete raw data and energy barrier results from both calculation methods to validate the reliability of our conclusions:

First, to more accurately simulate the kinetic response of the host framework during ion migration, we employed the all-atom NEB relaxation method and constructed a total of 11 structures for path sampling, including the initial state, nine intermediate transition states, and the final state. Compared to previous calculations (0.87eV, which used fewer transition state points), the more densely sampled energy barrier values obtained in this study are lower. This phenomenon is consistent with the fundamental principles of NEB calculations: a larger number of transition state points allows for a more accurate approximation of the true minimum energy path (MEP), thereby avoiding overestimation of the energy barrier caused by insufficient path

sampling (Figs. R3a and R3b). Nevertheless, the migration energy barrier of K-MnHCF remains significantly higher than K-HEHCF (0.32eV), and the core conclusion remains unchanged. Second, as a supplementary validation, we also employed the "frame-fixed approximation" method: during the NEB calculation, we fixed all frame atoms except for the migrating Na atom, allowing only the Na atom to relax. Under this method, with the force convergence criterion set to 0.05 eV/Å, the calculated migration energy barrier reached as high as 1.568 eV, and the energy curve was smooth with no abrupt changes (Figs. R3c and R3d). It should be noted that the rigid-framework approximation is a simplified computational method. Since it neglects the relaxation effects of the host framework, its results typically overestimate the true energy barrier for ion migration, a finding consistent with our computational results. It can be seen that, regardless of the calculation method used, the migration energy barrier of K-MnHCF is significantly higher than that of K-HEHCF. This core conclusion demonstrates a high degree of consistency and reliability. Compared to some other PBA studies, we used a larger number of transition states and a higher sampling density, resulting in greater accuracy (*Chemical Science, **2024**, 15, 11814-11824; Angew. Chem. Int. Ed. **2023**, 62, e202303953; Advanced Materials, **2025**, 37, 2417876*). When the atoms are not fixed, The process of Na^+ migration within the structure is shown in the Fig. R3e.

We have also uploaded the raw calculation files, output files, and fully optimized structures for both calculation methods to "DFT DATA" as Related Manuscript file for the manuscript to ensure the reproducibility and traceability of the calculation process.

Page 13, line 265 in manuscript, revised: "In addition, adsorption structure models for K-HEHCF and K-MnHCF were developed and optimized (see inset) to serve as a basis for calculating their adsorption energies, the calculated results are displayed in Fig. 3h."

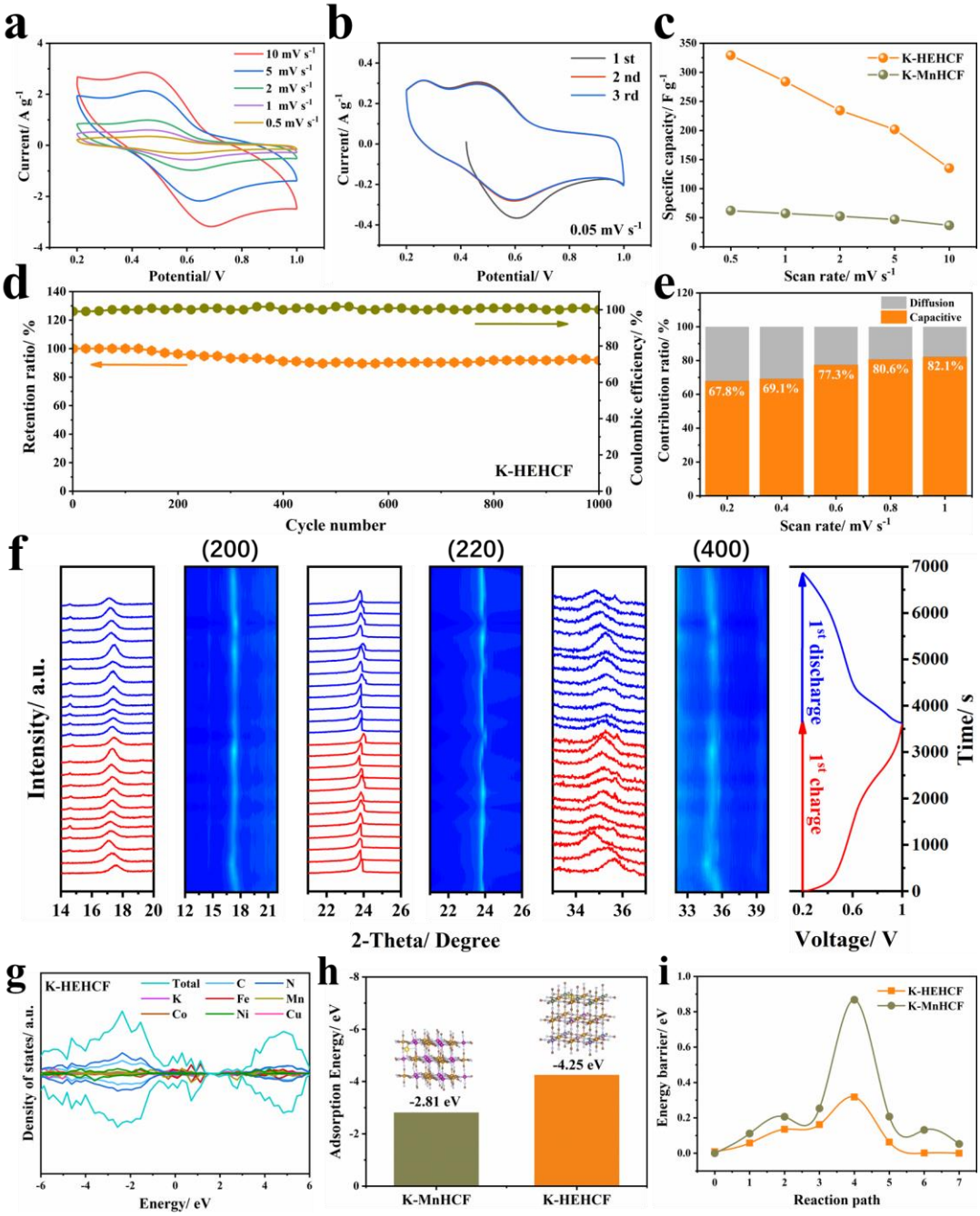

Fig. 3: Electrochemical properties and ion-capture mechanism of K-HEHCF. a CV curves of K-HEHCF at different scan rates. **b** CV curves for the first three cycles at a scan rate of 0.05 mV s^{-1}. **c** Comparison of Specific capacitance. **d** Cycling performance and coulombic efficiency at 2 A g^{-1} for 1000 GCD cycles. **e** The capacitive-controlled and diffusion-controlled contribution percentage of K-HEHCF. **f** Ex situ XRD patterns of K-HEHCF during the first cycle and corresponding charge/discharge curves. **g** Density of states of a K-HEHCF. **h** Calculation of the adsorption energy of Na on the HCFs surface. **i** The corresponding migration energy barriers for paths in different HCFs.

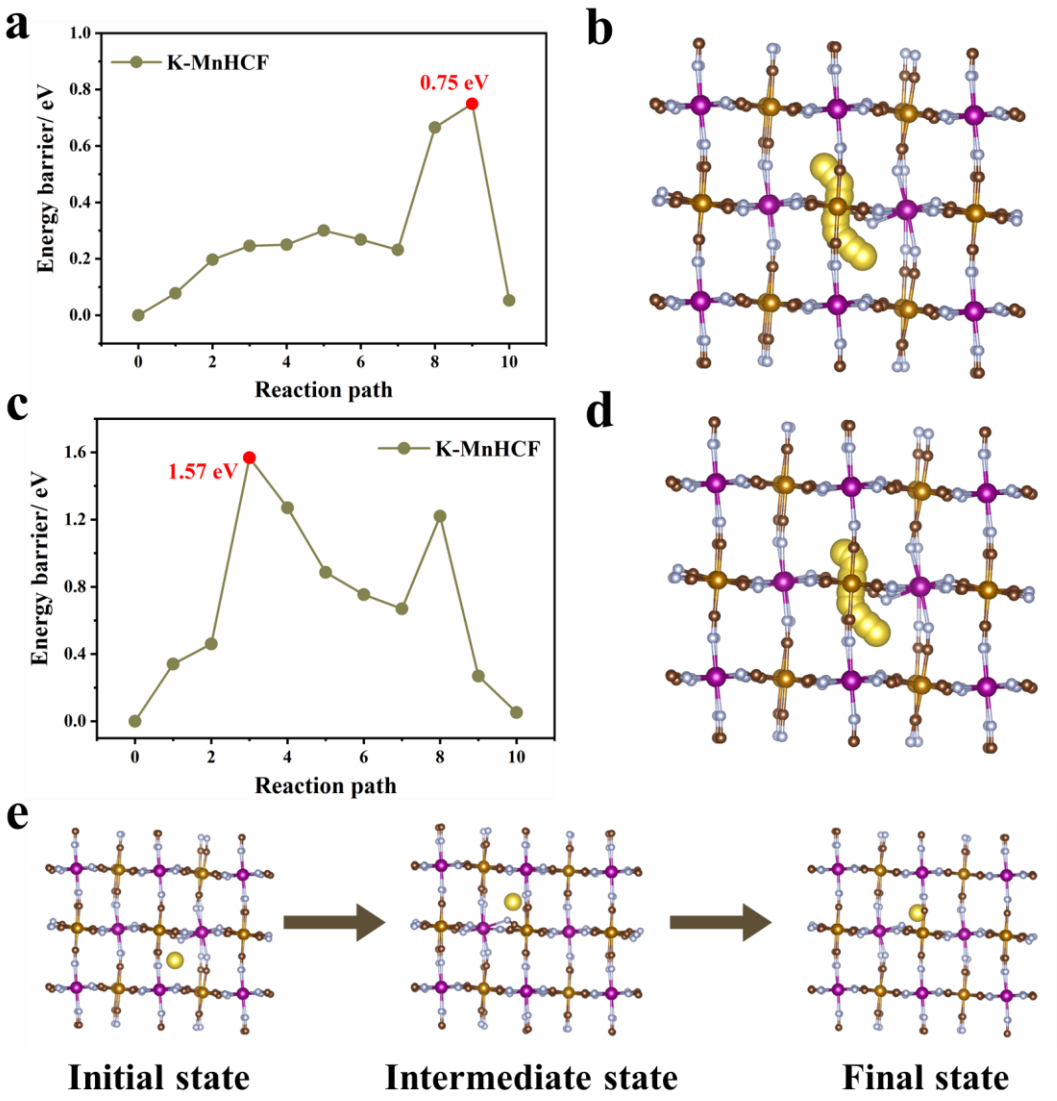

Fig. R3 (a) Migration energy barriers and (b) path for K-MnHCF with unfixed atoms.(c) Migration energy barriers and (d) path for K-MnHCF with fixed atoms. (e) Fully optimized atomic structures for initial, intermediate, and final configurations with non-fixed atoms.

Replies to the Reviewers' Comments

Thank you for your advice and guidance. We also would like to take this opportunity to thank the unnamed reviewers for their invaluable advice and suggestions on our work. We have revised the manuscript following the suggestions from the reviewers. Below are our response and answers to the reviewers' comments and questions on our manuscript (**NCOMMS-25-83721**). Our response to reviewer comments will be in blue color and the revised parts in red color, which are highlighted in yellow color in the revised Manuscript and Supplementary Information.

We hope that our responses to the comments and the revised manuscript will meet with approval.

Reviewer: #1

COMMENTS TO AUTHOR:

This manuscript describes the design and electrochemical investigation of a K^+-substituted high-entropy Prussian blue analogue (K-HEHCF) for enhanced capacitive deionization and energy recovery applications. The authors systematically analyze the structural stabilization effects induced by both high configurational entropy and K^+ substitution, demonstrating improved water resistance, lattice stability, and energy recovery efficiency compared to conventional HEHCFs. The manuscript is well organized, and the experimental data are comprehensive and clearly presented.

Response: We thank the reviewer for the valuable comments and suggestions. All the concerns raised from the reviewer have been addressed in detail as follows.

1. While the manuscript is well executed, the originality of the work is somewhat limited. The authors have previously reported a high-entropy PBA system in Advanced Science (2024) (Ref. 35), and the present study appears to be an extension of that concept through the incorporation of K^+ substitution. However, the effects of K^+ ions on PBA frameworks—such as water-content reduction, structural stabilization, and partial ion-exchange behavior—have already been well documented in the literature. In particular, K^+-substituted HE-PBAs have recently been reported in Desalination (617 (2026) 119487). Therefore, the distinct contribution of this study should be more clearly emphasized.

Response: We sincerely appreciate the reviewer's detailed comments on the innovative aspects of this work. We fully acknowledge that high entropy PBA materials and K substitution strategies have established research foundations in relevant fields.

However, this work is not merely an extension of K substitution based on our earlier HE-PBA design, but rather the first systematic coupling of the high entropy concept with precise K^+ regulation within the CDI field. It jointly reveals the synergistic enhancement mechanism between the two from multiple dimensions, including water content, ion diffusion kinetics, cycling stability, and capacitance contribution mechanisms. Simultaneously, it thoroughly explores the advantages of K substitution for Na and the storage mechanism of Na ions.

The unique and novel contributions of this work, compared with existing literature, are highlighted as follows:

First, unlike single high entropy strategies or isolated K^+ substitution, this work demonstrates for the first time the synergistic effect of high entropy configurations and K^+ substitution, simultaneously achieving low defect density, low water content, high stability, and high-rate capacitive behavior (*Angewandte Chemie Int. Ed* ***2023****, 62, e202303953*).

Second, it systematically elucidates the stabilization mechanism of K^+ regulation in high entropy PBA frameworks, clarifying its unique role in suppressing lattice collapse, reducing water content, enhancing ion transport, and facilitating reversible adsorption-desorption (*Desalination* ***2026****, 617, 119487*).

Third, most reported studies on high entropy PBAs have focused on a single cation system, with few comprehensive and systematic comparisons between K^+ and Na^+-based PBAs. Through this direct comparative experiment, our work clearly demonstrates that K^+ substitution is key to further enhancing the desalination performance of high entropy PBAs, constituting a significant innovation and highlight that distinguishes this research from existing literature.

Page 5, line 90 in manuscript, added: "Recent reports on high entropy PBAs research have mostly focused on a single cation system or remained limited to comparisons with low entropy PBAs, demonstrating improved CDI performance. However, comprehensive and systematic comparisons between K^+ and Na^+-based PBAs have been scarce."

2. The manuscript frequently attributes the superior performance of K-HEHCF to the synergistic effect between high configurational entropy and K^+ incorporation. However, this synergy has not been rigorously validated, as the two factors are not experimentally decoupled.

Response: Thank you for your professional comments. The outstanding performance of K-HEHCF stems from the combined effects of K substitution and configuration entropy. We supplemented the CV testing of Na-MnHCF and calculated its specific capacitance, revealing that K-MnHCF exhibits superior capacitive performance compared to Na-HEHCF (Supplementary Figs. 14 and 15). Furthermore, combined with the cyclability and water content tests of Na- and K-based PBAs supplemented in Comment 3, it can be observed that K substitution exerts a positive influence on the structure of HCFs. However, the limitations of single-metal-site persist. At this point, we introduce the concept of high entropy, incorporating multiple metallic elements into PBAs. Leveraging the inherent high stability of high configurational entropy and the "cocktail effect", we couple this with the low water content and low lattice defect advantages achieved through K substitution. This synergistic approach delivers a significant enhancement in the performance of K-HEHCF. As shown in Fig. R1, the CDI curves indicate that the MnHCF phase after K substitution exhibits reduced side reactions compared to Na-MnHCF, yet its adsorption capacity remains poor. In contrast, the CDI process for K-HEHCF becomes normalized with excellent adsorption capacity. Therefore, we conclude that the synergistic effect of K substitution and the high entropy effect collectively endows K-HEHCF with its outstanding performance.

Page 9, line 188 in manuscript, revised: "The CV plot of K-MnHCF at the same scan rate is similar, but the redox peaks are not symmetrical (Supplementary Fig. 14a). The specific capacitance of K-MnHCF is slightly higher than that of Na-MnHCF, which may result from reduced lattice defects in MnHCF due to K substitution for Na (Supplementary Fig. 15)."

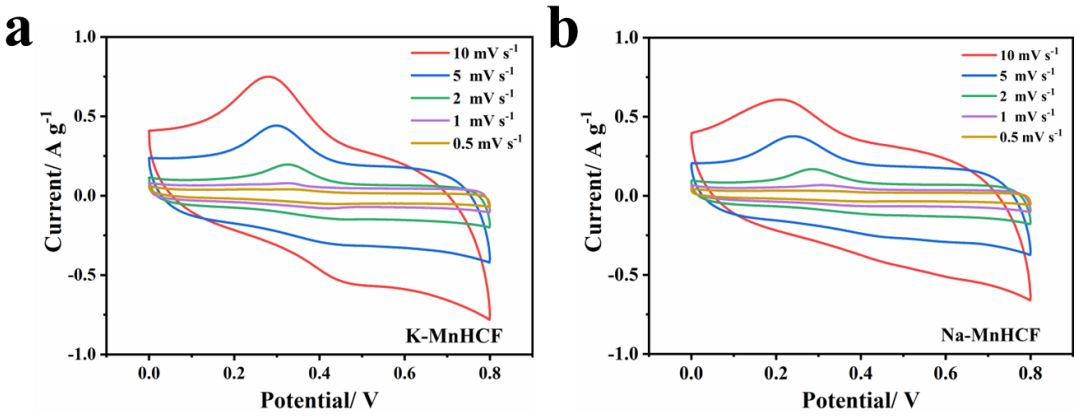

Supplementary Fig. 14 CV curves of (a) K-MnHCF and (b) Na-MnHCF at different scan rates.

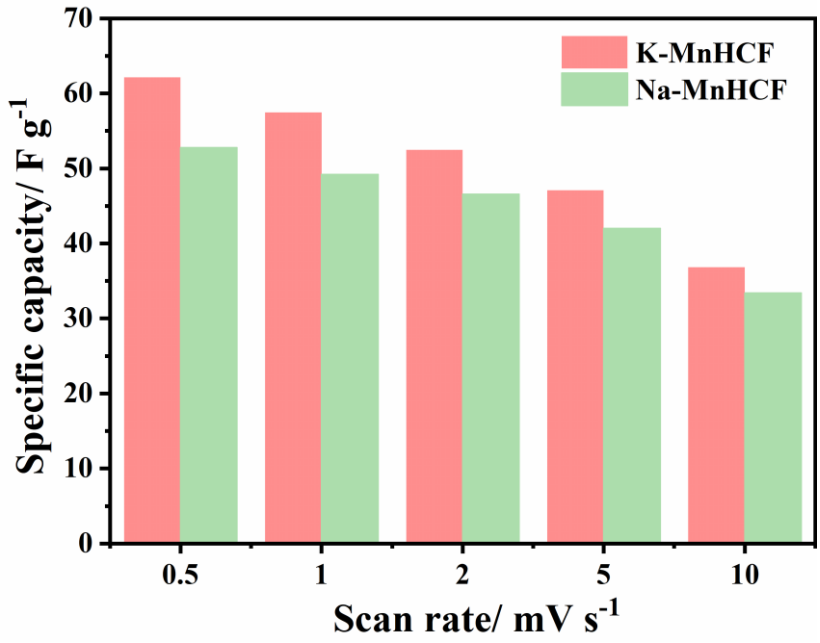

Supplementary Fig. 15 Comparison of Specific capacitance of (a) K-MnHCF and (b) Na-MnHCF.

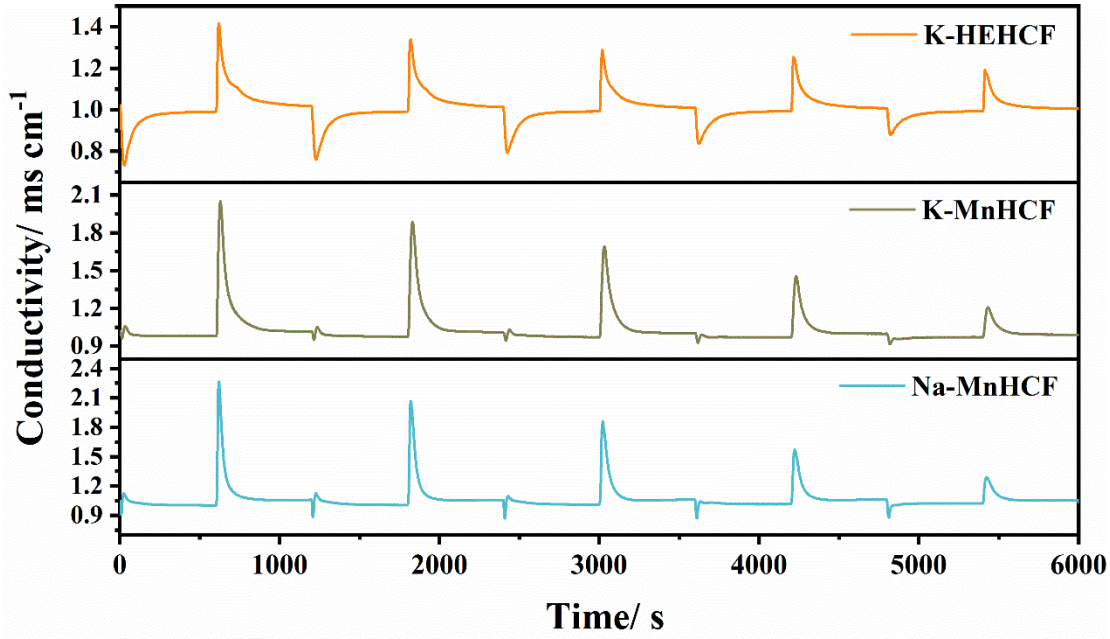

Fig. R1 CDI desalination curve for a NaCl solution with an initial concentration of 500 mg L^{-1}

3. To generalize the proposed mechanism, the authors are encouraged to compare the K^+ substitution behavior in other metal-centered PBAs (e.g., Co–HCF, Ni–HCF, or Fe–HCF). This would help clarify whether the observed "pillar effect" and water-content suppression are universal phenomena or specific to Mn-based systems.

Response: Many thanks for your insightful comments. Following the reviewer's suggestion, we synthesized HCFs with other single-metal-center elements besides Mn (Fe-HCF, Co-HCF, Ni-HCF, and Cu-HCF). The XRD patterns are shown in Supplementary Figs. 31a-c. The results indicate that K-based PBAs exhibited superior capacity retention ratio compared to Na-based PBAs after 100 CDI cycles (Supplementary Figs. 31d-f). Additionally, we measured the K:Na atom ratio in K-HEHCF after different cycling cycles (Table R1), further validating the claim that incomplete exchange of Na and K ions occurs during cycling. The residual K^+ ions within the lattice can exert a "pillar effect" to stabilize the framework structure (Fig. 5b-g).

Thermogravimetric analysis (TGA) reveals the water content of different HCFs, with interstitial water content of K-based Fe-HCF, Co-HCF, Ni-HCF, and Cu-HCF being 5.26%, 2.93%, 6.87%, and 6.24%, respectively; while the coordinated water content was 4.43%, 0.64%, 1.17%, and 4.63%, respectively. In contrast, the interstitial water contents of Na-based Fe-HCF, Co-HCF, Ni-HCF, and Cu-HCF were 8.99%, 6.04%, 9.55%, and 6.94%, respectively; the coordinated water contents were 12.12%, 7.35%, 7.89%, and 11.87% (Fig. 32). These results align with those for HEHCFs and MnHCFs, indicating that K substitution effectively suppresses the water content of PBAs and reduces defect formation regardless of whether the center is polymetallic or monometallic.

In summary, the observed "pillar effect" and water-content suppression are universal phenomena. These interact synergistically with the high entropy strategy to enhance K-HEHCF, resulting in outstanding performance. This strategy establishes a new paradigm for synthesizing structurally stable, low-defect electrode materials that simultaneously exhibit high sodium storage efficiency.

Page 15, line 316 in manuscript, added: "Furthermore, cyclic stability testing and TGA of other single-metal-center PBAs also indicate that the mechanism underlying the superior performance of K-based PBAs over Na-based PBAs is not limited to Mn-based materials. The K-HEHCF material, synthesized by further coupling K substitution MnHCF with a high entropy strategy, exhibits outstanding electrochemical and desalination performance. This strategy provides a novel approach and design paradigm for constructing electrode materials with stable structures, low lattice defects, and high sodium-ion storage efficiency (Supplementary Figs. 31-32)."

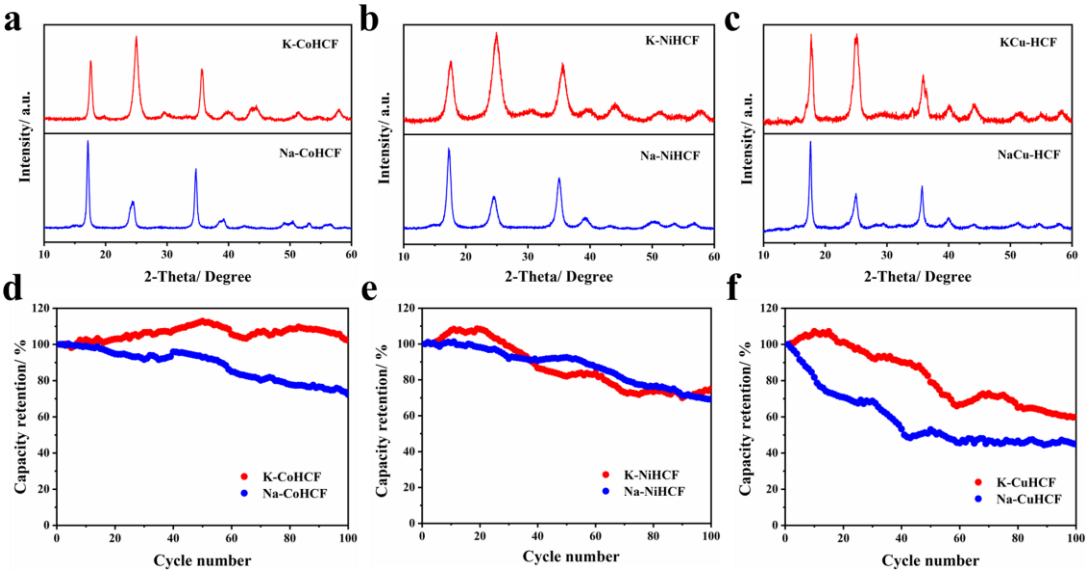

Supplementary Fig. 31 XRD patterns and capacity retention of other single metal-centered PBAs at 1 V.

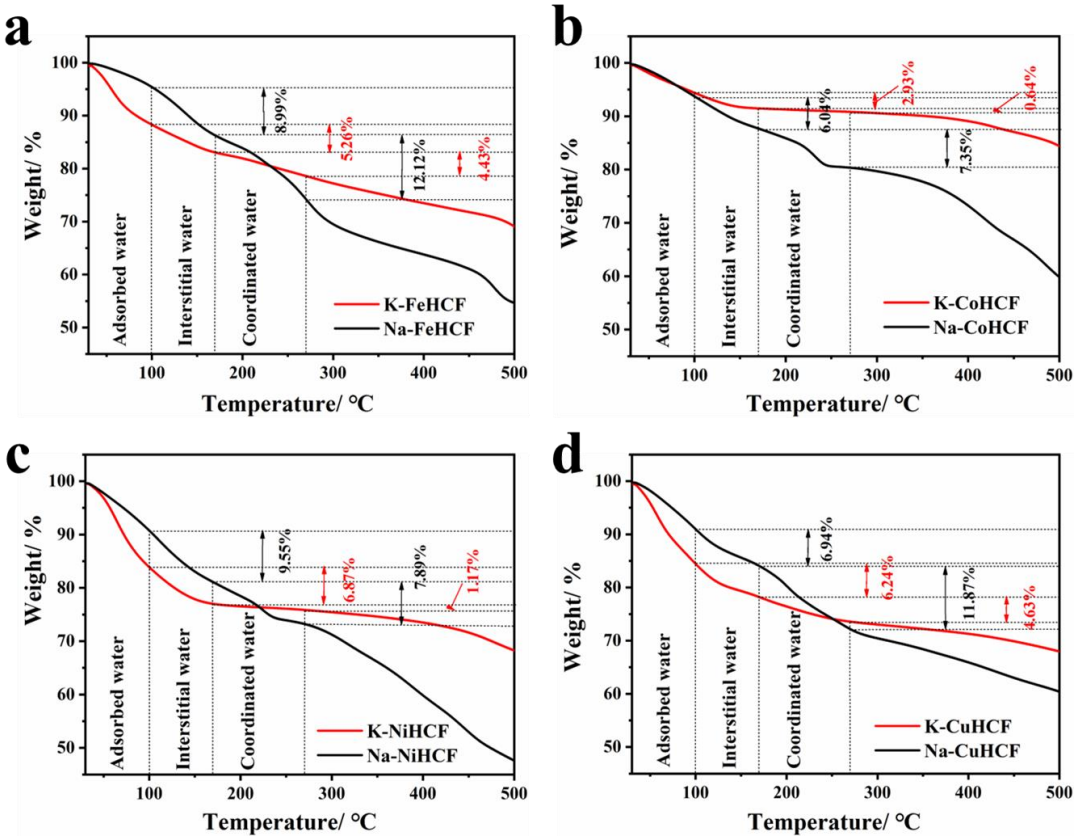

Supplementary Fig. 32 TGA curves of (a) FeHCFs, (b) CoHCFs, (c) NiHCFs and (d) CuHCFs.

Table R1. Atomic ratios of different elements in K-HEHCF after different cycles determined by XPS analysis.

Sample	Cycles	K/ at.%	Na/ at.%
K-HEHCF	0	11.31	0
	50	0.29	1.28
	100	0.32	1.09
	200	0.2	1.3

4. The CDI performance is impressive, but additional quantitative metrics are necessary to assess the practical feasibility of the proposed system. Specifically, the following data are recommended:

- Energy consumption per mole of salt removed (kWh mol^{-1} or kWh m^{-3}).
- Long-term electrode lifetime and structural stability beyond 200 cycles.
- Coulombic efficiency and true energy recovery ratio during charge/discharge cycles.

Response: Thank you very much for your pertinent comment. CDI performance stands as one of the most critical highlights in our work. Below, we provide a point-by-point explanation and supplement regarding the aspects raised in the comments.

First, we recalculated the molar energy consumption of K-HEHCF and Na-HEHCF at different voltages, with results shown in Supplementary Fig. 30. The energy consumed by K-HEHCF samples during CDI was significantly lower than that of Na-HEHCF, particularly at the selected optimal voltage of 1.4 V. This low energy consumption is more conducive to practical applications, as mentioned in our article, the K substitution strategy significantly enhances the desalination capacity of HEHCF.

Second, the long-term cycling performance of electrode materials is undeniably crucial for the practical application of CDI. Therefore, we conducted CDI cycling tests on K-HEHCF for up to 200 cycles. The results demonstrated that the cycle retention rate remained above 95%, fully validating the importance of high configurational entropy in suppressing unfavorable phase transitions during the reaction process. Furthermore, we compared the CDI performance of K-HEHCF with that of the recently reported Faraday electrode material. It is evident that K-HEHCF significantly outperforms in terms of adsorption capacity and cycle life, clearly demonstrating its

excellent CDI performance and practical application potential. This sufficiently supports the core conclusions of this work. We will also conduct longer-cycle testing in future applied research (Fig. 4g and Supplementary Table 11).

Third, we calculated the coulombic efficiency and true energy recovery rate of K-HEHCF during CDI cycles. As shown in the figure, the decline in coulombic efficiency during the early cycling stage may be attributed to irreversible losses during electrode surface activation and increased hydrophilicity(*Advanced Materials* ***2023****, 35, 2210871; Journal of Materials Chemistry A* ***2015****, 3, 23864*). This process also corresponds to the enhanced desalination capacity of K-HEHCF in the early cycling phase (Figure 4f). As cycling progresses, the electrode system gradually achieves a stable adsorption-desorption equilibrium, with the coulombic efficiency stabilizing and maintaining above 90%, indicating excellent reversibility and structural stability of the electrode. Since the charge-discharge voltage during cycling is ±1 V, the calculated true energy recovery rate aligns with the coulombic efficiency (Supplementary Fig. 34).

Page 16, line 331 in manuscript, added: "As cycling progresses, the electrode system gradually achieves a stable adsorption-desorption equilibrium, with the coulombic efficiency stabilizing and maintaining above 90%, indicating excellent reversibility and structural stability of the electrode. Since the charge-discharge voltage during cycling is ±1 V, the calculated true energy recovery rate aligns with the coulombic efficiency (Supplementary Fig. 34)."

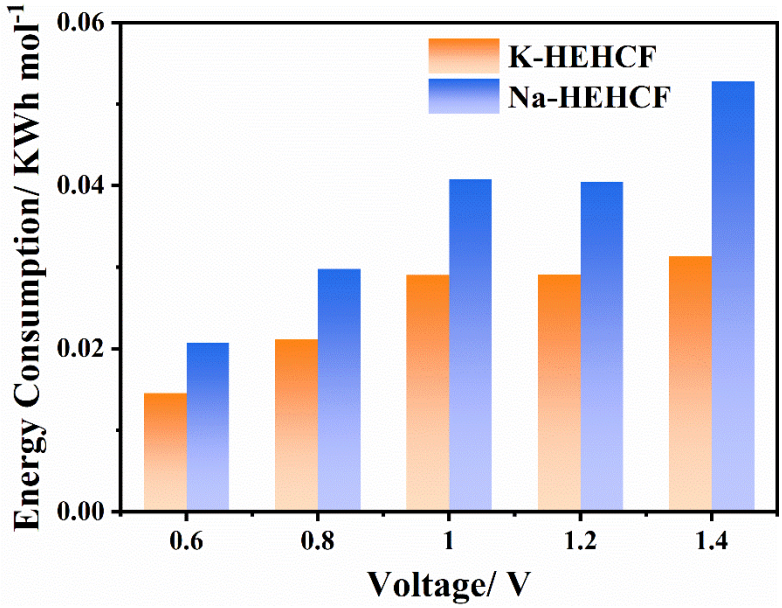

Supplementary Fig. 30 The energy consumption of K-HEHCF and Na-HEHCF at various voltage with 500 mg L^{-1} NaCl solution.

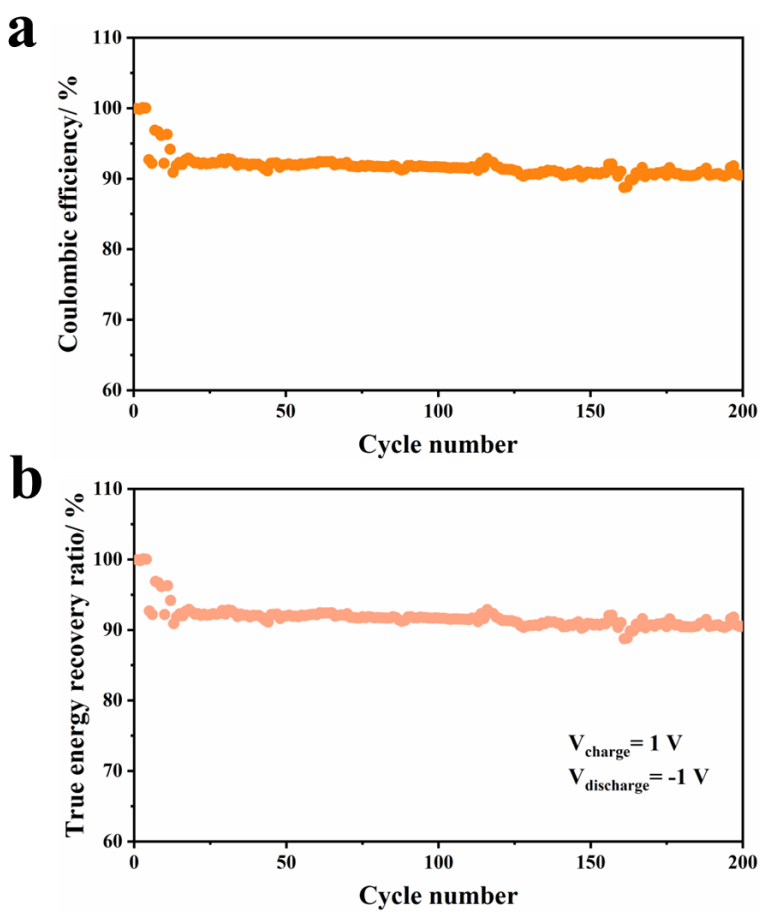

Supplementary Fig. 34 (a) Coulombic efficiency and (b) true energy recovery ratio during CDI cycles.

Reviewer: #2

COMMENTS TO AUTHOR:

In this manuscript, K-based high entropy hexacyanoferrate (K-HEHCF) is successfully synthesized by a one-step co-precipitation method. This electrode material can achieve good electrical conductivity and stability. The successful synthesis of the electrode material was demonstrated by various characterizations, and good desalination performance can be achieved in CDI applications. However, the experimental content of this manuscript is not novel enough, the materials are not innovative, so it cannot be accepted. The following are rejection reasons.

Response: We thank the reviewer for the valuable comments and suggestions. All the concerns raised from the reviewer have been addressed in detail as follows.

1. Please give the contents of different elements in K-HEHCF and Na-HEHCF to prove the mole fractions of the five elements are close to each other with about 0.2 using ICP and calculate the configuration entropy to ensure that ΔSconf > 1.5R.

Response: Thank you very much for your comments. The ICP-OES test results for K-HEHCF and Na-HEHCF are shown in Supplementary Table 1.

Supplementary Table 1 ICP-OES results of element ratios for K-HEHCF and Na-HEHCF.

Element	K	Fe	Mn	Co	Ni	Cu
Mole ratios	2.07	0.94	0.21	0.2	0.22	0.2

Element	Na	Fe	Mn	Co	Ni	Cu
Mole ratios	3.02	0.75	0.24	0.22	0.18	0.19

Calculate the configuration entropy of K-HEHCF and Na-HEHCF according to equations 1-2 of the Methods.

$$\Delta S_{\mathrm{conf}} = -R\sum_{i=1}^{n} x_i \ln x_i \qquad (1)$$

$$\Delta S_{\mathrm{K-HEHCF}} = -R(0.17\ln 0.17 + 0.21\ln 0.21 + 0.2\ln 0.2 + 0.22\ln 0.22 + 0.2\ln 0.2) = 1.61R$$

$$\Delta S_{\mathrm{Na-HEHCF}} = -R(0.17\ln 0.17 + 0.24\ln 0.24 + 0.22\ln 0.22 + 0.18\ln 0.18 + 0.19\ln 0.19) = 1.60R$$

$\Delta S_{\mathrm{K-HEHCF}} > 1.5\mathrm{R}$, $\Delta S_{\mathrm{Na-HEHCF}} > 1.5\mathrm{R}$.

The computational results indicate that the configuration entropies of both K-HEHCF and Na-HEHCF exceed 1.5 R, placing them within the high entropy category. **Page 6, line 119 in manuscript**, revised: "ICP-OES results indicate that the main transition metal elements in K-HEHCF are Fe, Mn, Co, Ni, and Cu, and the mole fractions of the five elements are close to each other with about 0.2. The ΔS_{conf} can be determined using the definitions derived from statistical thermodynamics, based on the Eqs. 1-2, we can calculate the ΔS_{conf} of K-HEHCF as 1.61R, which exceeds 1.5R and reaches high entropy category (Supplementary Table 1)."

2. The pseudo-capacitance calculation results of electrochemical tests show that the capacitance contribution rate of K-HEHCF increases from 34.4% to 81.6%. Why does this part of the data show that the proportion of capacitance is relatively small? Please explain and modify it. Please re-select the small sweep speed range and calculate the capacitance contribution more convincingly.

Response: Thank you for your comments. During CV testing in the manuscript, I employed scanning rates ranging from 0.5 to 10 mV s^{-1}. Using these CV curves, I calculated the capacitive contribution via Dunn's method, which increased from 34.4% at 0.5 mV s^{-1} to 81.6% at 10 mV s^{-1}. However, as you mentioned, the early capacitive contribution calculated at higher scan rates is relatively low, ions struggle to diffuse sufficiently into the active sites within the material in a short time, leading to diffusion-controlled processes dominating the reaction. To obtain a more reliable contribution ratio for the dynamics, calculations were re-performed within the low scan rate range of 0.2-1.0 mV s^{-1}, the percentage contribution from capacitance increased from 67.8% at 0.2 mV s^{-1} to 82.1% at 1 mV s^{-1} (Fig. 3e and Supplementary Fig. 19). At low scan rates, ion diffusion and charge transfer processes become more thorough, significantly enhancing the proportion of capacitive control and improving its authenticity. The rapid charge-discharge capability of K-HEHCF electrodes facilitates efficient and stable capacitive deionization behavior.

Page 11, line 216 in manuscript, revised: "To obtain a more reliable kinetic contribution ratio, we performed calculations using a low scanning rate range of 0.2-1.0 mV s^{-1}. After calculation, the b values of the two peak currents of K-HEHCF are 0.95 and 0.94 respectively (Supplementary Fig. 18)."

Page 11, line 220 in manuscript, revised: "It can be observed that the capacitive contribution increases with the increase in scan rate, from 67.8% at 0.2 mV s^{-1} to 82.1%

at 1 mV s^{-1} (Fig. 3e and Supplementary Fig. 19), indicating that the ion/charge migration is mainly controlled by capacitive control."

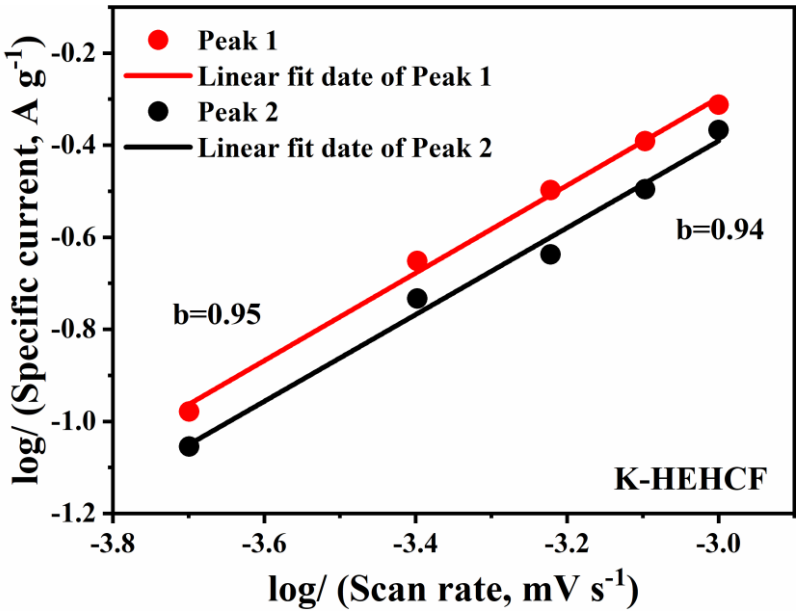

Supplementary Fig. 18 Linear correlation between the logarithmic peak current and sweep rate of K-HEHCF.

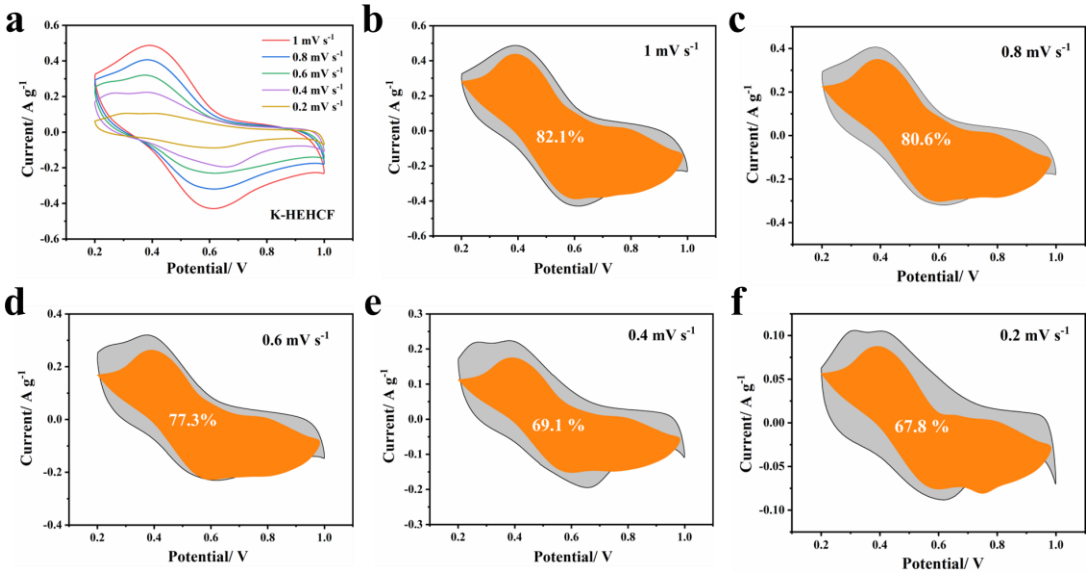

Supplementary Fig. 19 The contribution of capacitive-controlled (color) and diffusion-controlled process (grey) of K-HEHCF at different scan rates.

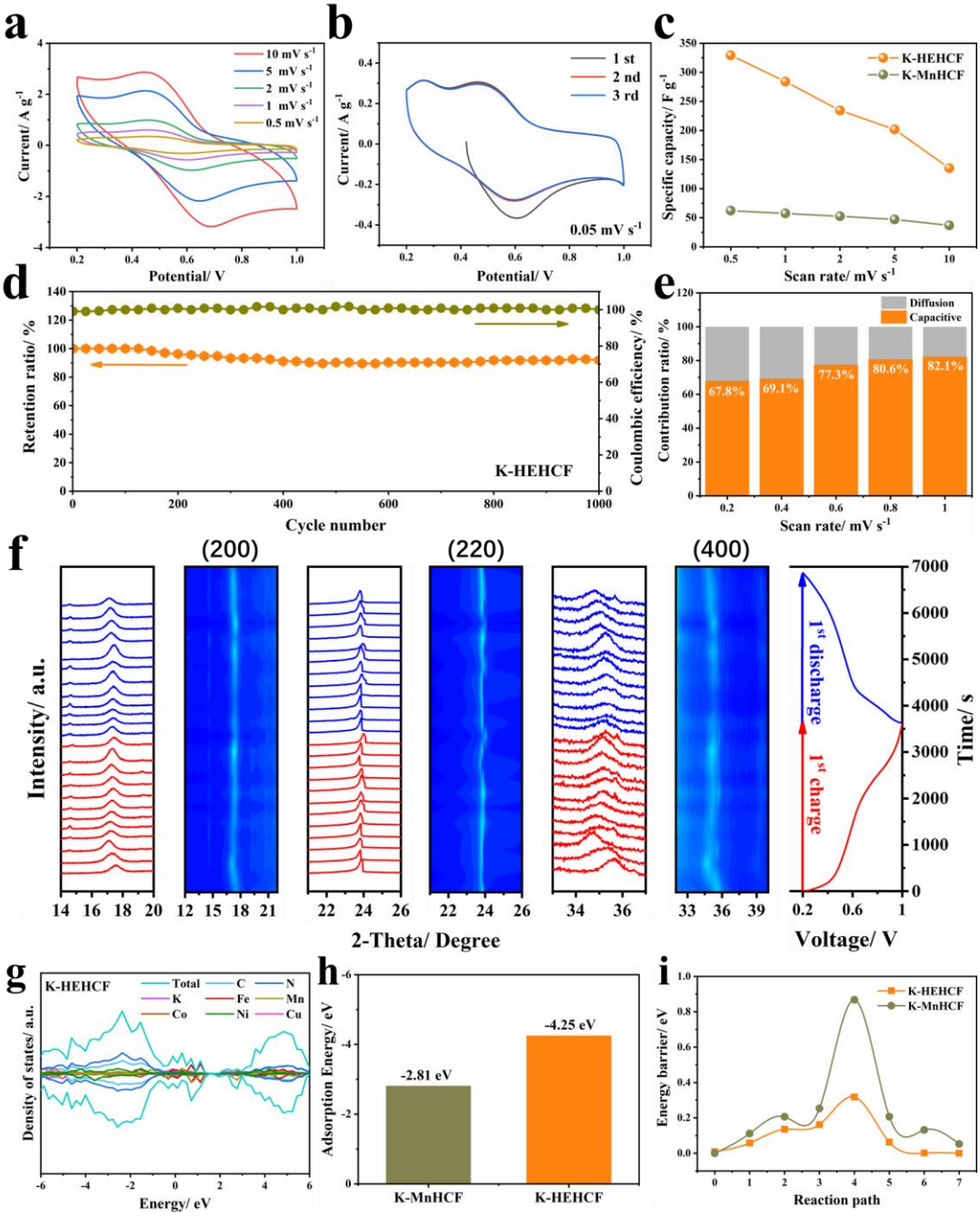

Fig. 3: Electrochemical properties and ion-capture mechanism of K-HEHCF. a CV curves of K-HEHCF at different scan rates. **b** CV curves for the first three cycles at a scan rate of 0.05 mV s^{-1}. **c** Comparison of Specific capacitance. **d** Cycling performance and coulombic efficiency at 2 A g^{-1} for 1000 GCD cycles. **e** The capacitive-controlled and diffusion-controlled contribution percentage of K-HEHCF. **f** Ex situ XRD patterns of K-HEHCF during the first cycle and corresponding charge/discharge curves. **g** Density of states of **a** K-HEHCF. **h** Calculation of the adsorption energy of Na on the HCFs surface. **i** The corresponding migration barrier energies for paths in different HCFs.

3. Why the K-HEHCF have good removal efficiency for the common multivalent salt ions, especially for Ca^{2+}?

Response: Thanks for your invaluable suggestions. As you can see, we designed a multi-channel tandem CDI system with five treatment units (Figure S33) to treat simulated circulating cooling water. The coupled CDI system exhibited excellent mixed-ion separation performance in the simulated circulating cooling water. The Ca and Mg ions in the treated simulated circulating cooling water were almost negligible, especially for Ca^{2+}.

This is mainly due to the following reasons:

First, the application of CDI technology for the selective extraction of different ions from saltwater has been reported for some time, and He et al. (*Environmental Science & Technology* ***2018****, 52, 9350-9360; Separation and Purification Technology* ***2022****, 280, 119828; Advanced Functional Materials* ***2021****, 31, 2105203*) have achieved the selective removal of divalent Ca^{2+} and Mg^{2+} cations compared with monovalent Na^{+} by optimizing the operating conditions in the face of high hardness brackish water, which provides us with theoretical support.

Second, there are specific ion exchange sites in the crystal structure of Prussian blue analogs, and the size, shape and charge distribution of these sites are selective for the exchange of different ions. The size and charge distribution of multivalent ions may be better suited for these exchange sites, for example, Zhao et al. (*Journal of Colloid and Interface Science,* ***2012****, 384, 38-44*) reported that in a typical capacitive deionization device, monovalent Na^{+} ions are initially adsorbed when a voltage difference is applied between the two electrodes, and are subsequently gradually replaced by divalent Ca^{2+} ions at lower concentrations. Therefore, after complete adsorption, K-HEHCF exhibits a preference for divalent ions in mixed ionic solutions, achieving highly efficient removal of Ca^{2+} and Mg^{2+}. In addition, from the energy point of view, the binding energy of multivalent ions with K-HEHCF is usually higher than that of Na^{+}. This means that the conjugates formed by Ca^{2+} and Mg^{2+} with K-HEHCF are more stable, and once Ca^{2+} and Mg^{2+} come into contact with and bind to K-HEHCF, they are not easy to be detached from the structure again, resulting in a higher selectivity and efficiency of Ca^{2+} and Mg^{2+} removal by K-HEHCF.

Third, from the perspective of diffusion speed, in general, the higher the charge density of an ion, the relatively slower its diffusion speed in solution. Since Na^{+} has a lower charge density and a smaller hydration radius, its diffusion speed in solution is

relatively faster, but this also makes its bonding with the surface of K-HEHCF relatively unstable, and it is easy to be detached again in the diffusion process. On the other hand, Ca^{2+} and Mg^{2+} have relatively slower diffusion speeds due to their higher charge density and larger hydration radius, but once they come into contact with the K-HEHCF surface, they are more inclined to be exchanged with and immobilized in the structure of K-HEHCF due to stronger electrostatic interactions, which improves the removal efficiency.

In summary, the removal efficiency of K-HEHCF for Ca^{2+} and Mg^{2+} ultimately exceeds that for Na^{+}, a result influenced by the combined effects of ion exchange thermodynamics, kinetics, and ion hydration radius.

Page 16, line 326 in manuscript, added: "In fact, numerous research studies have already investigated the feasibility of selectively extracting different ions from saltwater using CDI technology. Meanwhile, Prussian blue analogues such as K-HEHCF possess specific ion exchange sites within their crystal structures. The size, shape, and charge distribution of these sites confer selectivity toward different ions, with multivalent ions potentially exhibiting a more suitable size and charge distribution for these exchange sites. During adsorption, Na^{+} with lower charge density and smaller hydration radius typically adsorb preferentially due to their faster diffusion rate, but their binding is unstable. As adsorption approaches saturation, Ca^{2+} and Mg^{2+} with higher charge density and larger hydration radius are more readily attracted and fixed by the high charge density regions on the K-HEHCF surface. At this point, Na^{+} is often at a disadvantage in the adsorption competition and is eventually replaced by Ca^{2+} and Mg^{2+}. Consequently, K-HEHCF demonstrates excellent removal efficiency for Ca^{2+} and Mg^{2+}."

4. Please compare the contents of K and Na in materials before and after cycling to prove the exchange of K and Na during the reaction process. "Part of K^{+} will stay in K-HEHCF to be the backbone". Will this part K^{+} gradually decrease during long-term cycling, or will it remain in the material during long-term cycling? Please confirm it.

Response: Many thanks for your insightful comments about our manuscript. Upon initial analysis, we compared only the K^{+} content in K-HEHCF before and after the cycle to demonstrate that a small amount of K^{+} consistently remains throughout the process, exerting a "pillar effect". As requested by the reviewer, we have supplemented the data with the Na^{+} content changes in K-HEHCF during this process to confirm the

exchange of K and Na during the reaction (Supplementary Fig. 38). During the cycling process, the intensity of the K 2p characteristic peak from strong to weak, while the intensity of the Na 1s characteristic peak from absent to present, precisely confirming the exchange behavior between Na and K during this period.

We attempted to further confirm the Na^+/K^+ exchange of K-HEHCF during the charge-discharge process by 2D mapping spectra of TOF-SIMS. As seen in Figs. 5e-g, Na^+ was not present in the maps of the initial sample. However, from the maps of the sample after ten times of charging, it can be found that the Na^+ signals are obviously strengthened and the K^+ signals are weakened, indicating that Na^+ replaces part of the K^+ in the lattice, and the replaced K^+ is dissolved into the electrolyte. The sample maps after the subsequent discharge shows a reversible recovery of K^+, but not back to the initial strength, while the Na^+ signal strength continues to be strengthened. This may be due to the fact that the concentration of free Na^+ in the electrolyte is much higher than that of K^+, and the radius of Na^+ is smaller than that of K^+. In summary, K^+ and Na^+ undergo ion exchange during the reaction process, and the remaining K^+ is believed to be the backbone for reducing structural strain and stabilizing the framework, and may lead to long-term cycling performance.

Additionally, XPS analysis of K-HEHCF after different cycling cycles revealed a rapid decrease in K^+ content following reaction initiation, ultimately stabilizing at 0.2–0.3%. This process was accompanied by an increase and stabilization of Na^+, indirectly demonstrating that residual K^+ from the reaction remains stably present within K-HEHCF during long-term cycling and continues to exert its function (Table R1).

Page 17, line 351 in manuscript, revised: "As illustrated in Fig. 5b, the line-scan spectra of the K-HEHCF electrodes after CDI cycling showed significant K and Na signals, while the EDS spectra of K 2p also indirectly confirmed the residual of trace K^+ (Supplementary Fig. 37). Analysis of the evolution of high-resolution K 2p and Na 1s spectra before and after the K-HEHCF cycle further verifies the occurrence of reversible ion exchange between K^+ and Na^+(Supplementary Fig. 38)."

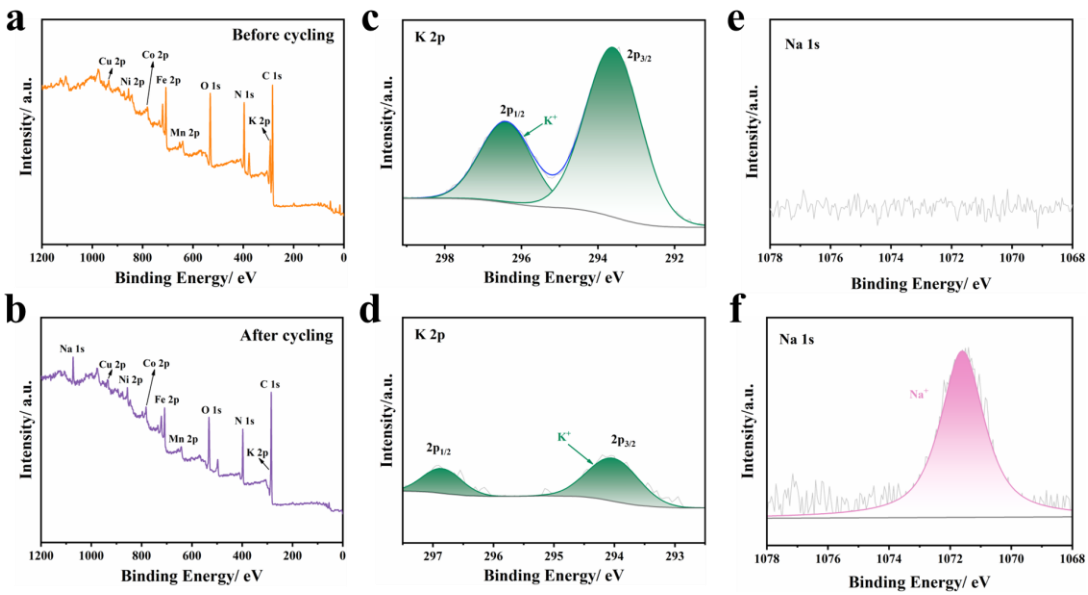

Supplementary Fig. 38 (a, b) XPS survey spectra, (c, d) K 2p and (e, f) Na 1s spectra of K-HEHCF before and after cycling.

Table R1. Atomic ratios of different elements in K-HEHCF after different cycles determined by XPS analysis.

Sample	Cycles	K/ at.%	Na/ at.%
K-HEHCF	0	11.31	0
	50	0.29	1.28
	100	0.32	1.09
	200	0.2	1.3

5. There are several similar published papers like https://doi.org/10.1021/acsnano.3c02323; https://doi.org/10.1007/s12274-022-5020-0; https://advanced.onlinelibrary.wiley.com/doi/10.1002/adfm.202510533.

Response: We thank the reviewer for the valuable comments and suggestions. The three works you mentioned are all outstanding and provide invaluable guidance for our subsequent research. Currently, the integration of the high entropy concept with Prussian blue has garnered increasing attention across various fields. This study differs from these previous works in the following aspects:

First, the aforementioned literature focuses on capacity, voltage optimization, and catalytic efficiency of energy storage batteries (Na-ion/ Zn-ion/ Li-CO_2 batteries). This work, however, targets enhancing the desalination performance of CDI, addressing the core challenge of achieving a balance between kinetics and high desalination capacity in CDI electrodes (*Coordination Chemistry Reviews* ***2024****, 520, 216100*).

Second, this work extends high entropy strategies and precise cation regulation to the CDI context, revealing their synergistic mechanism in enhancing desalination reversibility and kinetic performance. It establishes a new paradigm for cation design in CDI electrodes, distinct from the battery material optimization logic described in the aforementioned literature.

Third, the literature mentioned by the reviewer demonstrates performance optimization through a simple comparison between high entropy PBA and low or medium entropy PBAs, revealing a somewhat limited research perspective. In fact, as early as 2024, we proposed the core concept, reporting a high entropy Prussian blue analogue (HE-PBA) and systematically revealing the enhancement mechanism of high configurational entropy on the electrochemical performance of materials (*Advanced Science* ***2024****, 11, 2402340*). In this study, we did not confine ourselves to a single entropy engineering strategy. Instead, we achieved a critical expansion and performance upgrade of this concept through the innovative coupling of high entropy structures with K^+ substitution. Distinct from prior work, we conducted systematic comparative experiments between K^+- and Na^+-based PBAs across multiple core dimensions: crystalline water content, cycling stability, capacitive contribution mechanisms, and ion diffusion kinetics. This not only unequivocally demonstrated K ions significant structural and performance advantages but also elucidated its unique role in reducing lattice water content, enhancing ion adsorption capacity, suppressing structural distortion, and improving cycling reversibility. This provides a more comprehensive and targeted design approach for optimizing the performance of PBA-based electrode materials.

6. What is the mass of K-HEPBA and AC electrode respectively? In the desalination test, an area of 4.5*6.5 cm^2 is used, and the desalination performance test is greatly affected by the mass and area of the electrode, so please fully compare the desalination capacity of HEPBA with different mass and area.

Response: Thanks for the professional suggestion. The K-HEHCF and AC electrodes used in the CDI experiment weighed 32 – 36 mg each. They were fabricated by casting

a slurry mixture of active materials (AC, PBAs), carbon black, PVB, and PVP in a mass ratio of 8:1:1 onto graphite paper.

As the reviewer noted, desalination performance tests are significantly influenced by electrode mass and area. Therefore, to fully validate the optimal desalination performance of HEHCFs, we prepared three additional CDI electrodes with varying mass or area: 4.5×6.5 cm^2 graphite paper electrode with a mass ratio of 24:3:3, 4.5×6.5 cm^2 graphite paper electrode with a mass ratio of 40:5:5, and 5.5×7.5 cm^2 graphite paper electrode with a mass ratio of 32:4:4 (Fig. R1).

The results are shown in the Supplement Fig. 29. In a 500 mg/L NaCl solution, the same electrode exhibited differences in adsorption capacity depending on its mass and area. Among the combinations tested, the 32:4:4 ratio with a 4.5×6.5 cm^2 electrode used in the manuscript demonstrated the best performance.

Page 15, line 310 in manuscript, added: "It is worth noting that since desalination performance testing is significantly influenced by electrode mass and area, we additionally prepared three CDI electrodes with different masses or areas and tested them to fully validate the optimal desalination conditions for K-HEHCF. The results indicate that the electrode conditions employed in this experiment exhibit optimal desalination performance (Supplementary Fig. 29)."

Page 26, line 533 in manuscript, revised: "Subsequently, the resulting slurry of solids (32:4:4 mg) was cast on a graphite paper (4.5×6.5 cm^2) and then dried at 80 ℃ overnight."

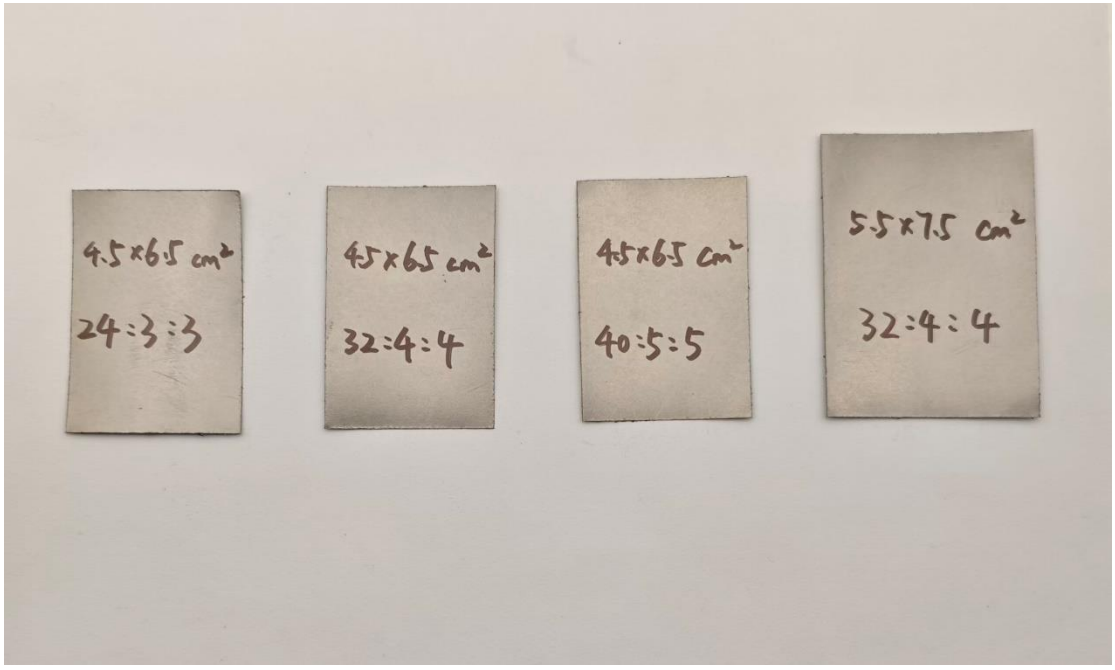

Fig. R1 Schematic diagram of CDI electrodes with different masses and areas.

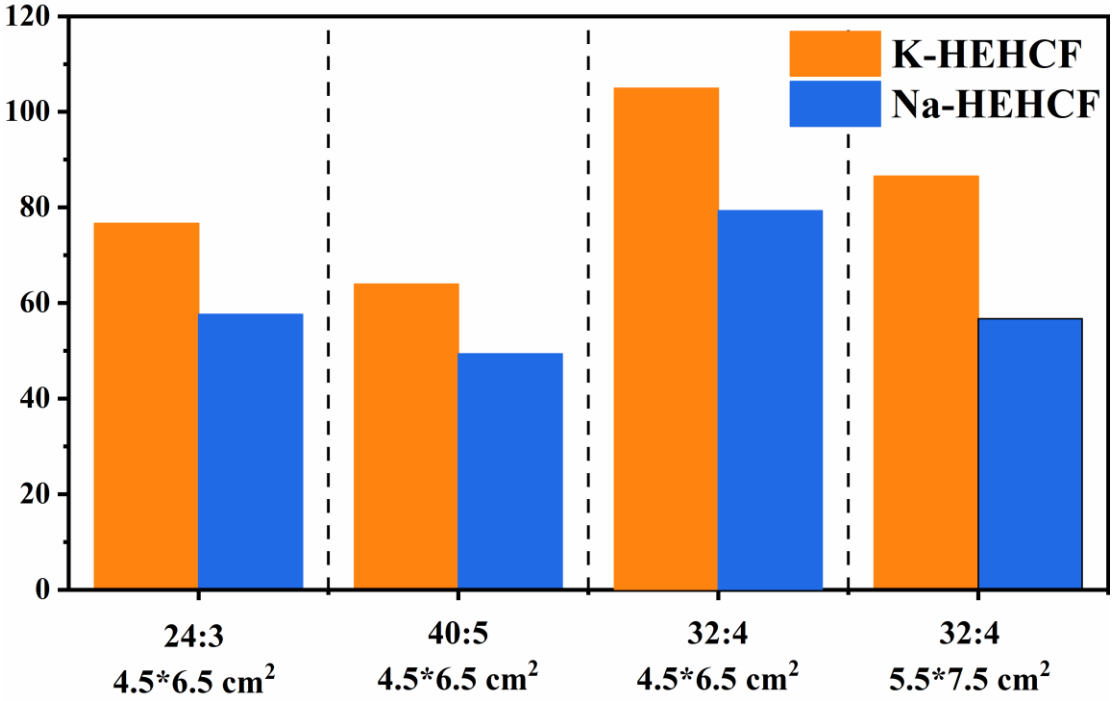

Supplementary Fig. 29 The adsorption capacity of K-HEHCF and Na-HEHCF at various conditions with 500 mg L^{-1} NaCl solution.

Replies to the Reviewers' Comments

On behalf of my co-authors, we thank you very much for giving us an opportunity to revise our manuscript. We would also like to once again thank the anonymous reviewers for their valuable suggestions and feedback on our research. We have revised the manuscript following the suggestions from the reviewers. Below are our response and answers to the reviewers' comments and questions on our manuscript (**NCOMMS-25-83721A**). Our response to reviewer comments will be in blue color and the revised parts in red color, which are highlighted in yellow color in the revised Manuscript and Supplementary Information.

We hope that our responses to the comments and the revised manuscript will meet with approval.

Reviewer: #1

COMMENTS TO AUTHOR:

The manuscript has been revised satisfactorily in accordance with the comments. It may be accepted for publication in Nature Communications.

Response: I would like to express my sincere gratitude for the many insightful professional comments and constructive suggestions you have provided. Your thoughtful feedback has greatly enhanced the quality of our paper, and we sincerely appreciate the effort and dedication you have shown throughout the review process.

Reviewer: #2

COMMENTS TO AUTHOR:

Although the authors have addressed several previous comments, there remain significant concerns regarding the electrochemical characterization and computational analysis sections. These issues are fundamental and must be resolved before the manuscript can be considered for publication. The main reasons for rejection are outlined below:

Response: We thank the reviewer for the valuable comments and suggestions again. Those comments are all valuable and very helpful for revising and improving our paper. All the concerns raised from the reviewer have been addressed in detail as follows.

1. According to the Methods section, the cyclic voltammetry (CV) measurements were conducted using a three-electrode system in 1 M NaCl, with scans performed from low to high voltage. However, in Figures 3a and 3b, the positions of the oxidation and reduction peaks are reversed compared with those reported in previous publications on HEPBA and PBA materials. Please clarify and explain this discrepancy. Furthermore, in Figure 3f, the galvanostatic charge–discharge (GCD) curve shows the oxidation peak as higher than the reduction peak, which is inconsistent with the CV profiles. please provide a clear explanation of this inconsistency and verify the accuracy of electrochemical data.

Response: Thank you very much for your careful review of the electrochemical characterization section of this research paper and for your constructive feedback. Below, I will provide detailed clarifications and explanations regarding the issues you raised.

First, compared to previous reports on HEPBA and PBA materials, the differences in the positions of the redox peaks shown in Figs. 3a and 3b are due to variations in the experimental setup of the electrochemical workstation. As described in the experimental section, the electrochemical measurements were conducted using a three-electrode system with a CHI 760E electrochemical workstation (Shanghai CH Instruments Co., China) in a 1 M NaCl solution. The experimental parameters are shown in Fig. R1a, with the current polarity set to cathode positive. Under these conditions, the CV results shown in the manuscript can be obtained (Fig. R1b). When the current polarity is set to anodic positive, the same CV test is performed on K-HEHCF, and the resulting plots are illustrated in Figs. R1c – d. Although differences in

the configuration of the chemical workstation may result in variations in the visual order of the redox peaks, this does not alter the redox nature of the material itself. The CV curves exhibit excellent reproducibility in terms of peak current and shape characteristics, thereby confirming the reversible Na^+ insertion/extraction process in K-HEHCF.

Second, the GCD curve in Fig. 3f shows that the oxidation plateau is higher than the reduction plateau, but the CV curve exhibits a symmetrical redox peak. This is due to the asymmetry in polarization and ion diffusion. During the charging process (oxidation reaction), the material undergoes slight structural contraction and exhibits relatively low polarization, resulting in the formation of a stable high-potential plateau. During the discharge process (reduction reaction), the material undergoes structural expansion, accompanied by slight kinetic hindrance, causing the working potential to decrease slightly, which makes the reduction plateau appear lower than the oxidation plateau. This kinetic asymmetry during charging and discharging is common and does not contradict the reversible redox peaks observed in the CV curve (*Chemical Science, **2024**, 15, 11814-11824; PNAS, **2026**, 123, e2525797123; Angewandte Chemie Int. Ed, **2025**, 64, e202501797*). The same GCD test was performed on three parallel samples of K-HEHCF at a current density of 1 A g^{-1}, as seen in the Fig. R2. It can be observed that, although there are slight differences in the charge and discharge times due to variations in the active mass of the electrodes, the shape of the curves remains unchanged, with the oxidation plateau being slightly higher than the reduction plateau, consistent with the results reported in the manuscript. Furthermore, the midpoint potential of the voltage plateau in the GCD curve corresponds to the average potential of the oxidation and reduction peaks in the CV curve, confirming that the redox potentials reflected by the two testing techniques are identical.

In summary, the observed differences are attributable to the current polarity settings and the kinetic asymmetry during the charging and discharging processes, rather than experimental errors or data inconsistencies. All electrochemical test results are reliable and chemically sound.

Page 9, line 183 in manuscript, revised: "The cyclic voltammetry curves of K-HEHCF are depicted in Fig. 3a, which exhibits a pair of distinct redox peaks in the 0.4-0.8 V range, which corresponded to the intercalation and deintercalation of Na^+ in the electrode, respectively."

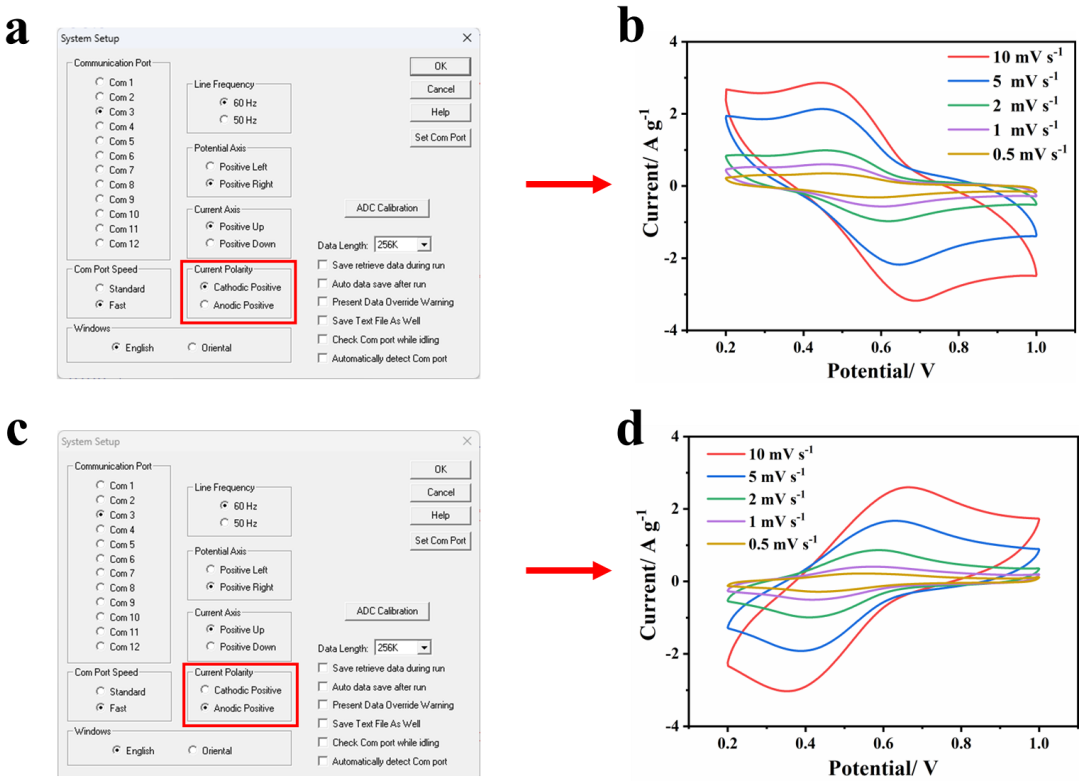

Fig. R1 (a, b) The experimental setup used in the manuscript and the resulting CV curves. (c, d) The modified experimental setup and the resulting CV curve.

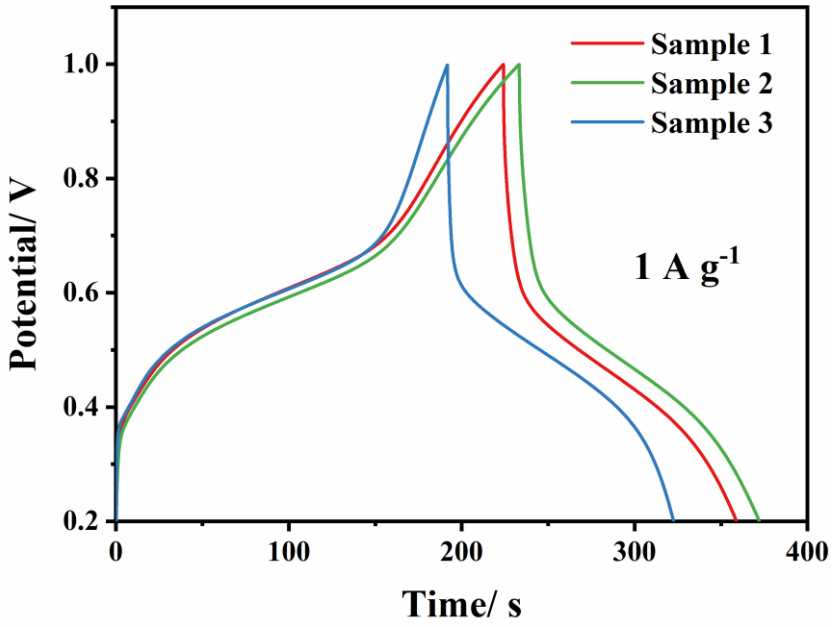

Fig. R2 GCD curves of K-HEHCF parallel samples at 1 A g^{-1}.

2. The manuscript lacks a dedicated Methods section describing the density functional theory (DFT) calculations. To ensure reproducibility and technical reliability, please add detailed information on the computational approach used. In addition, the raw

computational input files and key output files should be provided for all critical points and transition states discussed in the text.

Response: Thank you for your comments. A description of the density functional theory (DFT) computational method has been added to the Methods section. In addition, we have uploaded the raw computational files and key output files as Related Manuscript file under the filename "DFT DATA".

Page 26, line 529 in manuscript, added: "The computational analysis was carried out based on density functional theory (DFT) calculations, as implemented in Vienna ab initio simulation packages (VASP). The projector augmented wave (PAW) scheme and Perdew-Burke-Ernzerhof functional was used for geometric optimizations. In the geometric optimization, all atoms were allowed to relax until the calculated Hellmann-Feynman forces smaller than 0.03 eV/Å. The kinetic energy cutoff of 520 eV was chosen for the plane wave expansion."

3. For the adsorption energy study shown in Figure 5h, the optimized adsorption structure of Na-PBA should be provided. Regarding Figure 5i, the current number of images used is insufficient to accurately fit the reaction pathway, particularly for the green line. The authors should recompute the results using an adequate number of intermediate states and include the corresponding energy barrier values along with fully optimized atomic structures for the initial, intermediate, and final configurations.

Response: Thanks for your invaluable suggestions. We provide the optimized adsorption structures of K-HEHCF and K-MnHCF in the file and have inserted them as illustrations in Fig. 3h. In addition, we have provided further details regarding the NEB transition state calculations for the ion migration process of the green line (K-MnHCF), and have included the complete raw data and energy barrier results from both calculation methods to validate the reliability of our conclusions:

First, to more accurately simulate the kinetic response of the host framework during ion migration, we employed the all-atom NEB relaxation method and constructed a total of 11 structures for path sampling, including the initial state, nine intermediate transition states, and the final state. Compared to previous calculations (0.87eV, which used fewer transition state points), the more densely sampled energy barrier values obtained in this study are lower. This phenomenon is consistent with the fundamental principles of NEB calculations: a larger number of transition state points allows for a more accurate approximation of the true minimum energy path (MEP), thereby avoiding overestimation of the energy barrier caused by insufficient path

sampling (Figs. R3a and R3b). Nevertheless, the migration energy barrier of K-MnHCF remains significantly higher than K-HEHCF (0.32eV), and the core conclusion remains unchanged. Second, as a supplementary validation, we also employed the "frame-fixed approximation" method: during the NEB calculation, we fixed all frame atoms except for the migrating Na atom, allowing only the Na atom to relax. Under this method, with the force convergence criterion set to 0.05 eV/Å, the calculated migration energy barrier reached as high as 1.568 eV, and the energy curve was smooth with no abrupt changes (Figs. R3c and R3d). It should be noted that the rigid-framework approximation is a simplified computational method. Since it neglects the relaxation effects of the host framework, its results typically overestimate the true energy barrier for ion migration, a finding consistent with our computational results. It can be seen that, regardless of the calculation method used, the migration energy barrier of K-MnHCF is significantly higher than that of K-HEHCF. This core conclusion demonstrates a high degree of consistency and reliability. Compared to some other PBA studies, we used a larger number of transition states and a higher sampling density, resulting in greater accuracy (*Chemical Science, **2024**, 15, 11814-11824; Angew. Chem. Int. Ed. **2023**, 62, e202303953; Advanced Materials, **2025**, 37, 2417876*). When the atoms are not fixed, The process of Na^+ migration within the structure is shown in the Fig. R3e.

We have also uploaded the raw calculation files, output files, and fully optimized structures for both calculation methods to "DFT DATA" as Related Manuscript file for the manuscript to ensure the reproducibility and traceability of the calculation process.

Page 13, line 265 in manuscript, revised: "In addition, adsorption structure models for K-HEHCF and K-MnHCF were developed and optimized (see inset) to serve as a basis for calculating their adsorption energies, the calculated results are displayed in Fig. 3h."

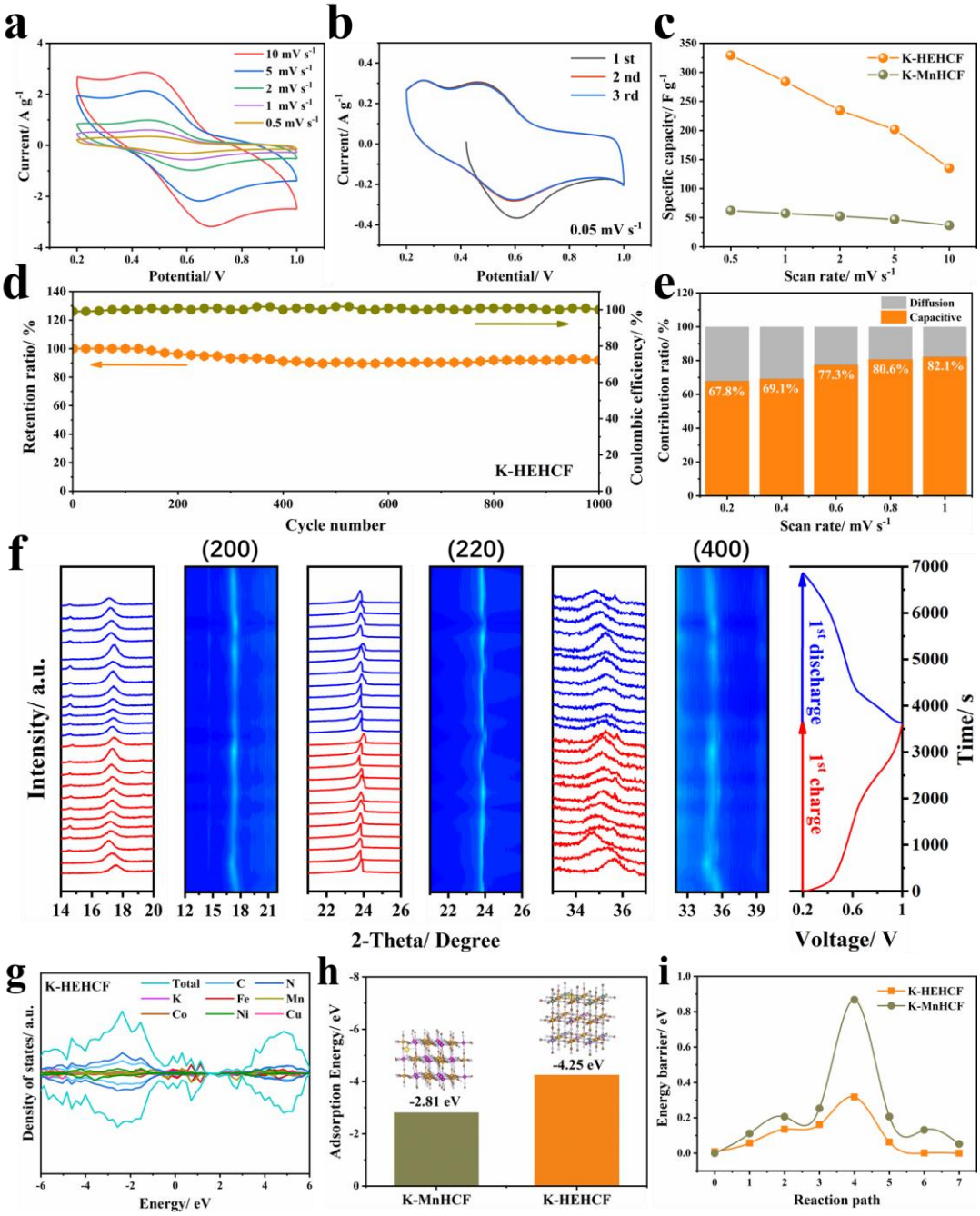

Fig. 3: Electrochemical properties and ion-capture mechanism of K-HEHCF. a CV curves of K-HEHCF at different scan rates. **b** CV curves for the first three cycles at a scan rate of 0.05 mV s^{-1}. **c** Comparison of Specific capacitance. **d** Cycling performance and coulombic efficiency at 2 A g^{-1} for 1000 GCD cycles. **e** The capacitive-controlled and diffusion-controlled contribution percentage of K-HEHCF. **f** Ex situ XRD patterns of K-HEHCF during the first cycle and corresponding charge/discharge curves. **g** Density of states of a K-HEHCF. **h** Calculation of the adsorption energy of Na on the HCFs surface. **i** The corresponding migration energy barriers for paths in different HCFs.

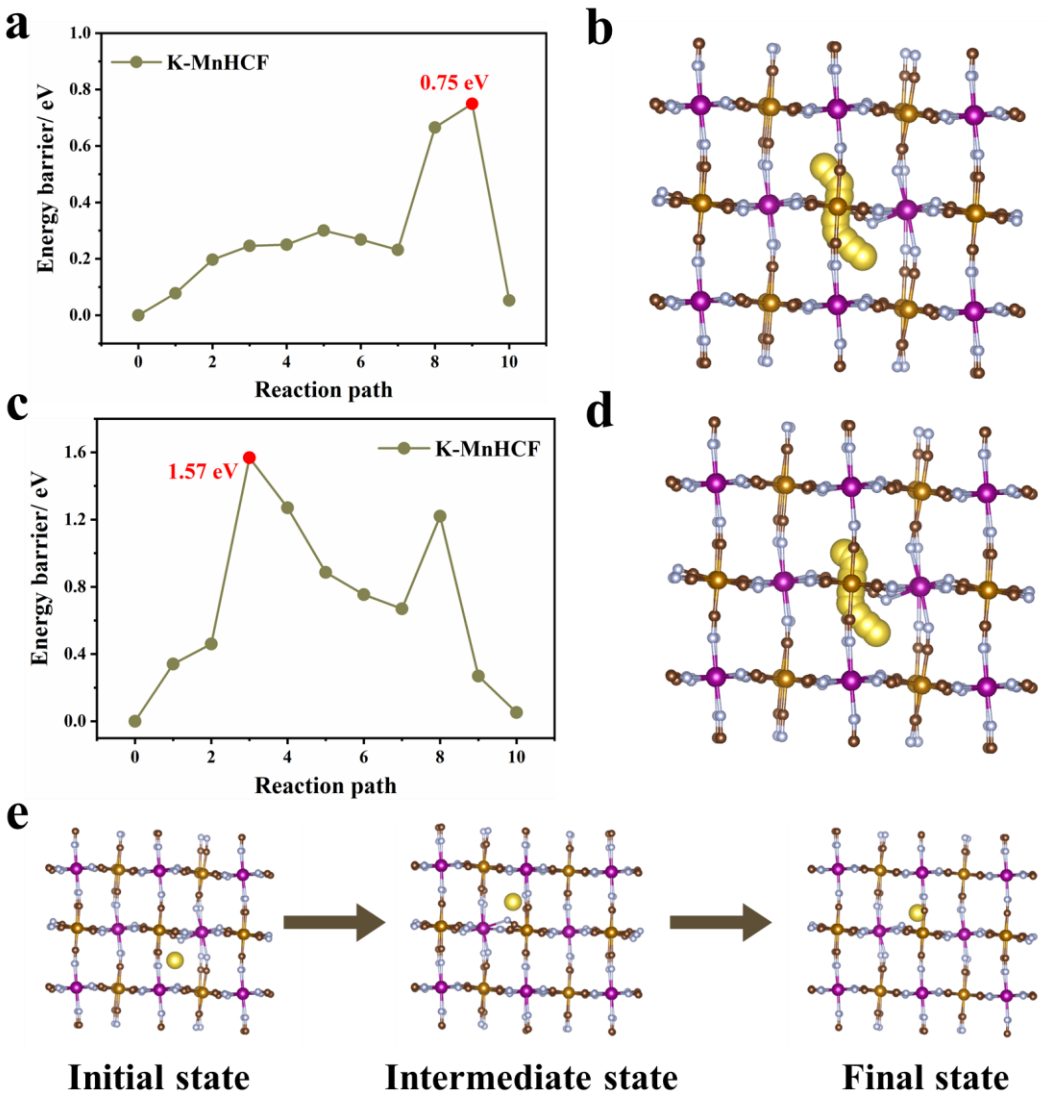

Fig. R3 (a) Migration energy barriers and (b) path for K-MnHCF with unfixed atoms.(c) Migration energy barriers and (d) path for K-MnHCF with fixed atoms. (e) Fully optimized atomic structures for initial, intermediate, and final configurations with non-fixed atoms.

Replies to the Reviewer' Comments

Below are our response and answers to the reviewers' comments and questions on our manuscript (**NCOMMS-25-83721B**).

Reviewer: #2

COMMENTS TO AUTHOR:

This manuscript has been revised thoroughly according to the provided comments, and it could be accepted for publication in Nature Communications.

Response: I would like to express my sincere gratitude for the many insightful professional comments and constructive suggestions you have provided. Your thoughtful feedback has greatly enhanced the quality of our paper, and we sincerely appreciate the effort and dedication you have shown throughout the review process.